

# Bloch Sphere of the Qutrit System

Surajit Sen<sup>†</sup> and Tushar Kanti Dey<sup>‡</sup>

Centre of Advanced Studies and Innovation Lab, 18/27 Kali Mohan Road,  
Tarapur, Silchar 788003, INDIA

<sup>†</sup>Corresponding Author: [ssen55@yahoo.com](mailto:ssen55@yahoo.com)

<sup>‡</sup>Email: [tkdey54@gmail.com](mailto:tkdey54@gmail.com)

## Abstract

We present a novel method to study the Bloch space of the qutrit system by examining the Bloch trajectories in it. Since such system is inherently a three-level quantum system, therefore we use the  $SU(3)$  group as the basis group to obtain the Bloch vectors of different configurations of it. The norm of the Bloch space is evaluated from the geometric consideration and also from the dynamics of the Bloch vectors and both results are found to be identical. The analysis of the dynamical evolution of the Bloch vectors reveals an additional feature that, under resonant conditions, the Bloch sphere  $S^7$  splits into two parts, a four-sphere  $S^4$  and a two-sphere  $S^2$ . The Bloch trajectories of the two sectors across different configurations exhibit a range of simple to complex curves, highlighting the non-trivial structure of the Bloch space of the qutrit system.

**Keywords:** Qutrit,  $SU(3)$  group, Three-level system, Bloch Sphere, Bloch trajectory

# 1 Introduction

The Bloch sphere representation is possibly the most elegant way of visualizing the state-space structure of the two-level quantum system [1]. Such system, which is commonly known as qubit, is geometrically represented by a unit two-sphere  $\mathbb{S}^2$  embedded in real three-dimensional space  $\mathbb{R}^{(3)}$  with poles  $|0\rangle$  and  $|1\rangle$  as its two principal cardinal states [1, 2]. All other states on the surface of the Bloch sphere can be built-up by the superposition of these cardinal states. Quantitatively, the Bloch sphere representation is characterized by the complex-valued density matrix operator [3, 4],

$$\rho_B = \frac{1}{2}(\sigma_0 + \mathbf{n}_B \cdot \boldsymbol{\sigma}), \quad \mathbf{n}_B \in \mathbb{R}^3 \quad (1)$$

where  $\sigma_0$  is the identity matrix and  $\sigma_i$  ( $i = 1, 2, 3$ ) represents the Pauli matrices. The Bloch vector of the qubit system  $\mathbf{n}_B$  appearing in Eq.(1) is defined as,

$$\mathbf{n}_B = \text{Tr}[\rho_B \boldsymbol{\sigma}], \quad n_1^2 + n_2^2 + n_3^2 = |\mathbf{r}_n|^2, \quad \mathbf{r}_n \in \mathbb{R}^3 \quad (2)$$

where the density matrix  $\rho_B$  satisfies the properties:  $\rho_B = \rho_B^\dagger$ ,  $\text{Tr}[\rho_B] = 1$ ,  $\rho_B^2 \geq 0$  [3, 5]. The properties of the Bloch vectors as well as the density matrix are consistent with the definition of *Purity* of the two-level system [3, 4],

$$\begin{aligned} \text{Tr}[\rho_B^2] &= \frac{1}{2}(1 + |\mathbf{r}_n|^2), \quad 0 \leq |\mathbf{r}_n|^2 \leq 1, \\ \frac{1}{2} &\leq \text{Tr}[\rho_B^2] \leq 1. \end{aligned} \quad (3)$$

In the realm of quantum information theory, the Bloch sphere plays very crucial role to elucidate different facets of the qubits such as, quantum gates and their operations, addressing measurement-related issues [2], studying the  $N$ -level systems known as qudits [6–10] and, most importantly, the entanglement scenario of the system with two or more qubits [11–15].

On the other hand, a qutrit system, the immediate generalization of a qubit, is inherently a three-level quantum system defined in Hilbert space  $\mathbb{H}^{(3)}$ . Since it is knitted with the foundational issues of the quantum mechanics in high-dimension, therefore recently considerable attention has been paid to visualize its Bloch sphere using different theoretical frameworks. These studies include, quaternion-inspired models [16], Heisenberg-Weyl methods [17, 18] and other approaches [5, 19–22]. Apart from them, recently there has been growing interest to construct the Bloch sphere for the qutrit system using  $\text{SU}(3)$  group because of its innate simplicity, rich underlying symmetry and close analogy with the qubit system [5, 8, 23–25]. In spite of some

progress, these methods become quite complex due to the limited information available about the structure of its Bloch space. One possible way to simplify the complexity of the qutrit system is to evaluate the Bloch vectors from using a dynamical approach. This method involves solving the Schrödinger equation for the three-level system and then construct the Bloch vectors from its solution. Implementing this method requires using all possible configurations of the three-level system which are categorized into three types:  $\Lambda$ ,  $V$ , and  $\Xi$  configurations. These models have been extensively studied in recent years and applied to address a wide variety of quantum optical systems [25–32]. In this paper, we analyze the properties of the Bloch space for each configuration by examining the phase space trajectories of the Bloch vectors, which we will refer to as  $SU(3)$  Bloch vectors, and demonstrate how this approach captures the nuances and subtleties of the Bloch sphere that may not be evident through other methods.

The remaining sections of this paper are structured as follows: In Section II, we consider the standard parametrization scheme of the qutrit system in terms of the spherical polar coordinates from the geometric consideration and obtain the norm of the Bloch space. We then discuss the cardinal states of the system and obtain all possible superposed states from them. Since the qutrit system is essentially a three-level system at the heart, therefore in Section III, we give detailed evaluation of the  $SU(3)$  Bloch vectors from the dynamical consideration while taking account of all configurations allowed by the selection rule. In Section IV, we analyze the Bloch trajectories of different configurations from their phase space portraits and discuss their behaviour both at resonance and off-resonance. Finally, we conclude by summarizing the essential content of the paper and discuss the outlook.

## 2 Qutrit system

### 2.1 Cardinal states of qutrit system

The wave function of a qutrit system can be written in the standard basis,

$$|\psi_T\rangle = c_1 |1\rangle + c_2 |2\rangle + c_3 |3\rangle, \quad (4)$$

where the basis states are given by,

$$|1\rangle = \begin{pmatrix} 1 \\ 0 \\ 0 \end{pmatrix}, \quad |2\rangle = \begin{pmatrix} 0 \\ 1 \\ 0 \end{pmatrix}, \quad |3\rangle = \begin{pmatrix} 0 \\ 0 \\ 1 \end{pmatrix}, \quad (5)$$

and the normalized complex amplitudes are parameterized as,

$$c_1 = \cos \frac{\theta_1}{2}, \quad (6a)$$

$$c_2 = e^{i\phi_1} \sin \frac{\theta_1}{2} \sin \frac{\theta_2}{2}, \quad (6b)$$

$$c_3 = e^{i\phi_2} \sin \frac{\theta_1}{2} \cos \frac{\theta_2}{2}, \quad (6c)$$

with range,  $\{\theta_i\} \in [0, \pi]$  and  $\{\phi_i\} \in [0, 2\pi)$  ( $i = 1, 2$ ). The density matrix read off from the qutrit wave function Eq.(4) is given by,

$$\rho_T = \begin{bmatrix} \cos^2 \frac{\theta_1}{2} & \frac{1}{2} e^{i\phi_1} \sin \theta_1 \sin \frac{\theta_2}{2} & \frac{1}{2} e^{i\phi_2} \sin \theta_1 \cos \frac{\theta_2}{2} \\ \frac{1}{2} e^{-i\phi_1} \sin \theta_1 \sin \frac{\theta_2}{2} & \sin^2 \frac{\theta_1}{2} \sin^2 \frac{\theta_2}{2} & \frac{1}{2} e^{-i(\phi_1 - \phi_2)} \sin^2 \frac{\theta_1}{2} \sin \theta_2 \\ \frac{1}{2} e^{-i\phi_2} \sin \theta_1 \cos \frac{\theta_2}{2} & \frac{1}{2} e^{i(\phi_1 - \phi_2)} \sin^2 \frac{\theta_1}{2} \sin \theta_2 & \sin^2 \frac{\theta_1}{2} \cos^2 \frac{\theta_2}{2} \end{bmatrix}, \quad (7)$$

which satisfies the idempotent condition,  $\rho_T^2 = \rho_T$ , giving the pure state condition,  $Tr[\rho_T^2] = 1$ .

Before addressing the norm of the Bloch space, we first consider the key cardinal states and their superposed states by the judicious choice of the coordinates. From Eqs.(4) and (5), the state vectors at some select location of the Bloch sphere are given by,

$$|\psi_T(\theta_1 = 0)\rangle = |1\rangle, \quad (8a)$$

$$|\psi_T(\theta_1 = \pi, \theta_2 = \pi)\rangle = e^{i\phi_1} |2\rangle, \quad (8b)$$

$$|\psi_T(\theta_1 = \pi, \theta_2 = 0)\rangle = e^{i\phi_2} |3\rangle, \quad (8c)$$

which may be referred as three principal cardinal states of the SU(3) Bloch space. Proceeding similar way, it is straight forward to obtain the superposition of these cardinal states,

$$|\psi_T(\theta_1 = \pi/2, \theta_2 = \pi)\rangle = \frac{1}{\sqrt{2}} [ |1\rangle + e^{i\phi_2} |2\rangle ], \quad (9a)$$

$$|\psi_T(\theta_1 = \pi, \theta_2 = \pi/2)\rangle = \frac{1}{\sqrt{2}} [ e^{-i\phi_1} |2\rangle + e^{-i\phi_2} |3\rangle ], \quad (9b)$$

$$|\psi_T(\theta_1 = \pi, \theta_2 = \pi/2)\rangle = \frac{1}{\sqrt{2}} [ |1\rangle - e^{i\phi_2} |3\rangle ], \quad (9c)$$

for any pair of states and

$$|\psi_T(\theta_1 = \pi/2, \theta_2 = \pi/3)\rangle = \frac{1}{\sqrt{2}} [ |1\rangle + \frac{1}{2} e^{i\phi_1} |2\rangle + \sqrt{\frac{3}{4}} e^{i\phi_2} |3\rangle ], \quad (10)$$

for all three states. The presence of such nontrivial states, unlike in the qubit system [1], is a primary signature of the complex dynamics of the SU(3) Bloch vectors of the qutrit system, which we will discuss by examining their Bloch trajectories.

## 2.2 SU(3) Bloch vectors from geometric consideration

The Bloch vectors for the qutrit system in the SU(3) basis is given by [5,33],

$$\mathbf{S}_T = Tr[\boldsymbol{\lambda}\rho_T], \quad \mathbf{S}_T \in \mathbb{R}^{(8)}, \quad (11)$$

where  $\rho_T$  be the density matrix of the qutrit system given by Eq.(7) and  $\lambda_i$  ( $i = 1, 2, \dots, 8$ ) be the GellMann matrices which in the qutrit basis are given by (including unit matrix  $\lambda_0$ ) [34],

$$\begin{aligned} \lambda_0 &= |1\rangle\langle 1| + |2\rangle\langle 2| + |3\rangle\langle 3|, & \lambda_1 &= |1\rangle\langle 2| + |2\rangle\langle 1| \\ \lambda_2 &= i[|2\rangle\langle 1| - |1\rangle\langle 2|], & \lambda_3 &= |1\rangle\langle 1| - |2\rangle\langle 2|, \\ \lambda_4 &= |1\rangle\langle 3| + |3\rangle\langle 1|, & \lambda_5 &= i[|3\rangle\langle 1| - |1\rangle\langle 3|], \\ \lambda_6 &= |2\rangle\langle 3| + |3\rangle\langle 2|, & \lambda_7 &= i[|3\rangle\langle 2| - |2\rangle\langle 3|], \\ \lambda_8 &= \frac{1}{\sqrt{3}}[|1\rangle\langle 1| + |2\rangle\langle 2| - 2|3\rangle\langle 3|]. \end{aligned} \quad (12)$$

The matrices are normalized as  $\lambda_l\lambda_m = \delta_{lm} + d_{lmn}\lambda_n + f_{lmp}\lambda_p$ , where  $d_{lmn}$  and  $f_{lmp}$  ( $l, m, n, p = 1, 2, \dots, 8$ ) are the completely symmetric and completely antisymmetric structure constants of the SU(3) group. It is straight forward to find the SU(3) Bloch vectors in terms of the angular parameters

by plugging in Eqs.(7) and (12) into Eq.(11),

$$S_{T_1} = \sin \theta_1 \sin \frac{\theta_2}{2} \cos \phi_1, \quad (13a)$$

$$S_{T_2} = -\sin \theta_1 \sin \frac{\theta_2}{2} \sin \phi_1, \quad (13b)$$

$$S_{T_3} = \cos^2 \frac{\theta_1}{2} - \sin^2 \frac{\theta_1}{2} \sin^2 \frac{\theta_2}{2} \quad (13c)$$

$$S_{T_4} = \sin \theta_1 \cos \frac{\theta_2}{2} \cos \phi_2, \quad (13d)$$

$$S_{T_5} = -\sin \theta_1 \cos \frac{\theta_2}{2} \sin \phi_2, \quad (13e)$$

$$S_{T_6} = \sin^2 \frac{\theta_1}{2} \sin \theta_2 \cos(\phi_1 - \phi_2), \quad (13f)$$

$$S_{T_7} = \sin^2 \frac{\theta_1}{2} \sin \theta_2 \sin(\phi_1 - \phi_2), \quad (13g)$$

$$S_{T_8} = \frac{1}{2\sqrt{3}} [(1 - 3 \cos \theta_2) + 3 \cos \theta_1 (1 + \cos \theta_2)], \quad (13h)$$

which follow the equation of seven-sphere  $\mathbb{S}^7$  embedded in the 8-dimensional Bloch space  $\mathbb{R}^8$ ,

$$S_{T_1}^2 + S_{T_2}^2 + S_{T_3}^2 + S_{T_4}^2 + S_{T_5}^2 + S_{T_6}^2 + S_{T_7}^2 + S_{T_8}^2 = \frac{4}{3}. \quad (14)$$

The reason for not scaling the Bloch vectors to have a unit sphere will become clear shortly.

## 3 SU(3) Bloch vectors from dynamical consideration

### 3.1 Three-level system revisited

To obtain the time-dependent SU(3) Bloch vectors, let us briefly recall dynamics of different configurations of the three-level system. The Hamiltonian of a generic three-level configuration ( $A = \Lambda, V, \Xi$ ) is given by [29, 33],

$$H^A(t) = H_0^A + H_I^A(t). \quad (15)$$

For the  $\Lambda$  configuration ( $A = \Lambda$ ), the unperturbed and interaction term of the Hamiltonian are given by,

$$H_0^\Lambda = \omega_{13}V_3 + \omega_{23}T_3 \quad (16a)$$

$$H_I^\Lambda(t) = \frac{1}{2}\kappa_{13}V^+e^{i\Omega_{13}t} + \frac{1}{2}\kappa_{23}T^+e^{i\Omega_{23}t} + h.c., \quad (16b)$$

where  $\omega_{ij} = |\omega_i - \omega_j|$  be the difference of energy between  $|i\rangle$ -th and  $|j\rangle$ -th level,  $\kappa_{ij}$  ( $i, j=1, 2, 3$  with  $i \neq j$ ) be the atom-field coupling parameters and  $\Omega_{ij}$  be the frequency of the external field. Similarly we have,

$$H_0^V = \omega_{13}V_3 + \omega_{12}U_3 \quad (17a)$$

$$H_1^V(t) = \frac{1}{2}\kappa_{13}V^+e^{i\Omega_{13}t} + \frac{1}{2}\kappa_{12}U^+e^{i\Omega_{12}t} + h.c., \quad (17b)$$

for the  $V$  configuration ( $A = V$ ) and

$$H_0^\Xi = \omega_{12}U_3 + \omega_{23}T_3 \quad (18a)$$

$$H_1^\Xi(t) = \frac{1}{2}\kappa_{12}U^+e^{i\Omega_{12}t} + \frac{1}{2}\kappa_{23}T^+e^{i\Omega_{23}t} + h.c. \quad (18b)$$

for the  $\Xi$  configuration ( $A = \Xi$ ). In defining above Hamiltonians, we have the following SU(3) shift operators [34],

$$\begin{aligned} T_+ &= |1\rangle\langle 2|, & T_- &= |2\rangle\langle 1| & T_3 &= |1\rangle\langle 1| - |2\rangle\langle 2| \\ V_+ &= |1\rangle\langle 3|, & V_- &= |1\rangle\langle 2| & V_3 &= |1\rangle\langle 1| - |3\rangle\langle 3| \\ U_+ &= |2\rangle\langle 3|, & U_- &= |3\rangle\langle 2|, & U_3 &= |2\rangle\langle 2| - |3\rangle\langle 3| \end{aligned} \quad (19)$$

which obey the following algebra,

$$\begin{aligned} [T^+, T^-] &= T^3 & [T^+, T^3] &= -2T^- & [T^-, T^3] &= 2T^+, \\ [V^+, V^-] &= V^3 & [V^+, V^3] &= -2V^- & [V^-, V^3] &= 2V^+, \\ [U^+, U^-] &= U^3 & [U^+, U^3] &= -2U^- & [U^-, U^3] &= 2U^+, \end{aligned} \quad (20)$$

and their operation on the basis states are given by,

$$\begin{aligned} T_+|1\rangle &= 0, & T_-|1\rangle &= |2\rangle & T_3|1\rangle &= |1\rangle, \\ T_+|2\rangle &= |1\rangle, & T_-|2\rangle &= 0 & T_3|2\rangle &= -|2\rangle, \\ T_+|3\rangle &= 0, & T_-|3\rangle &= 0 & T_3|3\rangle &= 0, \\ V_+|1\rangle &= 0, & V_-|1\rangle &= |3\rangle & V_3|1\rangle &= |1\rangle, \\ V_+|2\rangle &= 0, & V_-|2\rangle &= 0 & V_3|2\rangle &= 0, \\ V_+|3\rangle &= |1\rangle, & V_-|3\rangle &= 0 & V_3|3\rangle &= -|3\rangle, \\ U_+|1\rangle &= 0, & U_-|1\rangle &= 0 & U_3|1\rangle &= 0, \\ U_+|2\rangle &= 0, & U_-|2\rangle &= |3\rangle & U_3|2\rangle &= |2\rangle, \\ U_+|3\rangle &= |2\rangle, & U_-|3\rangle &= 0 & U_3|3\rangle &= -|3\rangle. \end{aligned} \quad (21)$$

Using the unitary matrix for the  $\Lambda$  configuration [33],

$$U_\Lambda(t) = \exp \left[ -\frac{i}{3} \left( (2\Delta_{13} - \Delta_{23})V_3t + (\Delta_{13} - 2\Delta_{23})T_3t \right) \right], \quad (22)$$

the Hamiltonian Eq.(16) can be expressed in the time-independent rotating frame [33],

$$\begin{aligned}\hat{H}_R^\Lambda(0) &= -i\dot{U}_\Lambda^\dagger(t)U_\Lambda(t) + U_\Lambda^\dagger(t)H^\Lambda(t)U_\Lambda(t) \\ &= \begin{bmatrix} \frac{1}{3}(\Delta_{13} + \Delta_{23}) & \kappa_{23} & \kappa_{13} \\ \kappa_{23} & \frac{1}{3}(\Delta_{13} - 2\Delta_{23}) & 0 \\ \kappa_{13} & 0 & -\frac{1}{3}(2\Delta_{13} - \Delta_{23}) \end{bmatrix}\end{aligned}\quad (23)$$

where the detuning offset are given by  $\Delta_{13} = 2\omega_{13} + \omega_{13} - \Omega_{13}$  and  $\Delta_{13} = 2\omega_{13} + \omega_{13} - \Omega_{13}$ . Finally taking equal-detuning condition, namely,  $\Delta_{13} = \Delta_{23} = \Delta$ , and making use of Equations (20) and (21), the Hamiltonian (23) leads to normalized amplitudes of the  $\Lambda$  configuration,

$$c_1(t) = e^{-\frac{1}{6}i\Delta t} \left\{ c_{10} \cos\left(\frac{\Omega t}{2}\right) - \frac{i}{\Omega} (c_{10}\Delta + c_{30}\kappa_{13} + c_{20}\kappa_{23}) \sin\left(\frac{\Omega t}{2}\right) \right\} \quad (24a)$$

$$\begin{aligned}c_2(t) &= \frac{e^{-\frac{1}{6}i\Delta t}}{(\kappa_{13}^2 + \kappa_{23}^2)\Omega} \left[ e^{\frac{1}{2}i\Delta t} \kappa_{13} (c_{20}\kappa_{13} - c_{30}\kappa_{23}) \Omega \right. \\ &\quad + \kappa_{23} (c_{30}\kappa_{13} + c_{20}\kappa_{23}) \Omega \cos\left(\frac{\Omega t}{2}\right) \\ &\quad \left. + i\kappa_{23} (c_{30}\Delta\kappa_{13} + c_{20}\Delta\kappa_{23} - c_{10}(\kappa_{13}^2 + \kappa_{23}^2)) \sin\left(\frac{\Omega t}{2}\right) \right] \quad (24b)\end{aligned}$$

$$\begin{aligned}c_3(t) &= -\frac{e^{-\frac{1}{6}i\Delta t}}{\kappa_{13}^2 + \kappa_{23}^2} \left[ e^{\frac{1}{2}i\Delta t} \kappa_{23} (-c_{20}\kappa_{13} + c_{30}\kappa_{23}) \right. \\ &\quad + \kappa_{13} (c_{30}\kappa_{13} + c_{20}\kappa_{23}) \cos^2\left(\frac{\Omega t}{2}\right) \\ &\quad \left. + i\kappa_{13} (c_{30}\Delta\kappa_{13} + c_{20}\Delta\kappa_{23} - c_{10}(\kappa_{13}^2 + \kappa_{23}^2)) \sin^2\left(\frac{\Omega t}{2}\right) \right], \quad (24c)\end{aligned}$$

where,  $\Omega = \sqrt{\Delta^2 + \kappa_{13}^2 + \kappa_{23}^2}$ .



### 3.2 $SU(3)$ Bloch vectors for $\Lambda$ -configuration

Taking analogy from Eq.(1) of the qubit system [4], we define the density matrix operator for the three-level system in the  $SU(3)$  basis,

$$\begin{aligned} \rho_{\text{TLS}}(t) &= \frac{1}{3} \left[ \boldsymbol{\lambda}_0 + \frac{3}{2} \mathbf{n}_T(t) \cdot \boldsymbol{\lambda} \right] \\ &= \begin{bmatrix} \frac{1}{6}(2 + 3n_3(t) + \sqrt{3}n_8(t)) & \frac{1}{2}(n_1(t) - in_2(t)) & \frac{1}{2}(n_4(t) - in_5(t)) \\ \frac{1}{2}(n_1(t) + in_2(t)) & \frac{1}{6}(2 - 3n_3(t) + \sqrt{3}n_8(t)) & \frac{1}{2}(n_6(t) - in_7(t)) \\ \frac{1}{2}(n_4(t) + in_5(t)) & \frac{1}{2}(n_6(t) + in_7(t)) & \frac{1}{3}(1 - \sqrt{3}n_8(t)) \end{bmatrix}, \end{aligned} \quad (25a)$$

where  $\mathbf{n}_T(t)$  is the  $SU(3)$  Bloch vector with the inner product defined as,

$$\begin{aligned} \mathbf{n}_T(t) \cdot \boldsymbol{\lambda} &= n_1(t)\lambda_1 + n_2(t)\lambda_2 + n_3(t)\lambda_3 + n_4(t)\lambda_4 \\ &\quad + n_5(t)\lambda_5 + n_6(t)\lambda_6 + n_7(t)\lambda_7 + n_8(t)\lambda_8. \end{aligned} \quad (25b)$$

Here we emphasize that the judicious choice of  $\frac{3}{2}$  in front of  $\mathbf{n}_T(t) \cdot \boldsymbol{\lambda}$  in Eq. (25a) rather than its other value discussed in the literature [5,23], ensures that the density matrix  $\rho_{\text{TLS}}$  gives precisely the same norm Eq. (14) obtained for the qutrit system. This establishes the complete equivalence between the qutrit system with the three-level system. Furthermore, from Eq. (25) it is easy to see that the *Purity* of such system can be related to the radius of the Bloch sphere [4,35],

$$\text{Tr}[\rho_{\text{TLS}}^2] = \frac{1}{3} \left( 1 + \frac{3}{2} |\mathbf{r}_T|^2 \right), \quad \mathbf{r}_T \in \mathbb{R}^8. \quad (26)$$

and we have a bound,

$$\frac{1}{3} \leq \text{Tr}[\rho_{\text{TLS}}^2] \leq 1, \quad 0 \leq |\mathbf{r}_T|^2 \leq \frac{4}{3} \quad (27)$$

where the lower bound corresponds to the maximally mixed state.

To describe the dynamical behavior of the  $SU(3)$  Bloch vectors, we consider the wave function of the three-level system,

$$|\psi^\Lambda(t)\rangle = c_1(t) |1\rangle + c_2(t) |2\rangle + c_3(t) |3\rangle, \quad (28)$$

and corresponding density matrix in terms of the time dependent amplitudes are given by,

$$\rho_{\text{TLS}}(t) = \begin{bmatrix} c_1^*(t)c_1(t) & c_1^*(t)c_2(t) & c_1^*(t)c_3(t) \\ c_2^*(t)c_1(t) & c_2^*(t)c_2(t) & c_2^*(t)c_3(t) \\ c_3^*(t)c_1(t) & c_3^*(t)c_2(t) & c_3^*(t)c_3(t) \end{bmatrix}. \quad (29)$$

Comparing Eq. (25) and Eq.(28), we obtain the desired time-dependent SU(3) Bloch vectors of a three-level configuration,

$$\mathbf{n}_T(t) = Tr[\boldsymbol{\lambda}\rho_{\text{TLS}}(t)], \quad (30)$$

where its components are given by,

$$\begin{aligned} n_1(t) &= c_1^*(t)c_2(t) + c_1(t)c_2^*(t), \\ n_2(t) &= i[c_1^*(t)c_2(t) - c_1(t)c_2^*(t)], \\ n_3(t) &= c_1^*(t)c_1(t) - c_3(t)c_3^*(t), \\ n_4(t) &= c_1^*(t)c_3(t) + c_1(t)c_3^*(t), \\ n_5(t) &= i[c_1^*(t)c_3(t) - c_1(t)c_3^*(t)], \\ n_6(t) &= c_2^*(t)c_3(t) + c_2(t)c_3^*(t), \\ n_7(t) &= i[c_2^*(t)c_3(t) - c_2(t)c_3^*(t)], \\ n_8(t) &= \frac{1}{\sqrt{2}}[c_1^*(t)c_1(t) + c_2^*(t)c_2(t) - 2c_3^*(t)c_3(t)]. \end{aligned} \quad (31)$$

For the  $\Lambda$  configuration, substituting the amplitudes Eq.(24) into (31) we obtain the corresponding SU(3) Bloch vectors (For detail, see Appendix-A). Furthermore, it readily gives the norm of the seven-sphere  $\mathbb{S}^7$  to be [33],

$$n_1^2(t) + n_2^2(t) + n_3^2(t) + n_4^2(t) + n_5^2(t) + n_6^2(t) + n_7^2(t) + n_8^2(t) = \frac{4}{3}. \quad (32a)$$

which exactly aligns with Eq.(14), as derived in Section II through geometrical considerations. In addition, in this dynamical approach we note that at the zero detuning condition ( $\Delta = 0$ ), the seven-sphere  $\mathbb{S}^7$  splits into two subspace: a four-sphere  $\mathbb{S}^4$  with the norms [33],

$$\begin{aligned} n_2^2(t) + n_3^2(t) + n_5^2(t) + n_6^2(t) + n_8^2(t) = \\ \frac{1}{3} \left[ -3c_{10}^{*2} (c_{20}^2 + c_{30}^2) + c_{20}^{*2} (4c_{20}^2 + 3c_{30}^2) \right. \\ \left. + 2c_{20}c_{20}^*c_{30}c_{30}^* + (3c_{20}^2 + 4c_{30}^2) c_{30}^{*2} + 2c_{10}c_{10}^* (c_{20}c_{20}^* + c_{30}c_{30}^*) \right. \\ \left. + c_{10}^2 (4c_{10}^{*2} - 3(c_{20}^{*2} + c_{30}^{*2})) \right], \end{aligned} \quad (32b)$$

and two-sphere  $\mathbb{S}^2$ ,

$$\begin{aligned} n_1^2(t) + n_4^2(t) + n_7^2(t) = c_{10}^{*2} (c_{20}^2 + c_{30}^2) - (c_{20}^*c_{30} - c_{20}c_{30}^*)^2 \\ + 2c_{10}c_{10}^* (c_{20}c_{20}^* + c_{30}c_{30}^*) + c_{10}^2 (c_{20}^{*2} + c_{30}^{*2}). \end{aligned} \quad (32c)$$

respectively. The procedure outlined above can be easily extended for the  $V$  and the  $\Xi$  configurations [33]. For the  $V$  configuration, we have the following norms,

$$n_1^{V^2}(t) + n_2^{V^2}(t) + n_3^{V^2}(t) + n_4^{V^2}(t) + n_5^{V^2}(t) + n_6^{V^2}(t) + n_7^{V^2}(t) + n_8^{V^2}(t) = \frac{4}{3}. \quad (33a)$$

Once again, at zero detuning condition ( $\Delta^V = 0$ ), the Bloch sphere split into two parts,

$$\begin{aligned} n_1^{V^2} + n_3^{V^2} + n_5^{V^2} + n_7^{V^2} + n_8^{V^2}(t) = \\ \frac{1}{3} [4c_{20}^2 c_{20}^{*2} - 3c_{20}^* c_{30}^2 + 3c_{10}^{*2} (c_{20}^2 - c_{30}^2) \\ + 2c_{20} c_{20}^* c_{30} c_{30}^* - 3c_{20}^2 c_{30}^{*2} + 4c_{30}^2 c_{30}^{*2} \\ + 2c_{10} c_{10}^* (c_{20} c_{20}^* + c_{30} c_{30}^*) + c_{10}^2 (4c_{10}^{*2} + 3c_{20}^{*2} - 3c_{30}^{*2})], \end{aligned} \quad (33b)$$

and,

$$\begin{aligned} n_2^{V^2}(t) + n_4^{V^2}(t) + n_6^{V^2}(t) = c_{10}^{*2} (-c_{20}^2 + c_{30}^2) + (c_{20}^* c_{30} + c_{20} c_{30}^*)^2 + \\ 2c_{10} c_{10}^* (c_{20} c_{20}^* + c_{30} c_{30}^*) + c_{10}^2 (-c_{20}^{*2} + c_{30}^{*2}). \end{aligned} \quad (33c)$$

Similarly for the  $\Xi$  configuration we have,

$$n_1^{\Xi^2}(t) + n_2^{\Xi^2}(t) + n_3^{\Xi^2}(t) + n_4^{\Xi^2}(t) + n_5^{\Xi^2}(t) + n_6^{\Xi^2}(t) + n_7^{\Xi^2}(t) + n_8^{\Xi^2}(t) = \frac{4}{3}, \quad (34a)$$

and at resonance ( $\Delta^\Xi = 0$ ) we have,

$$\begin{aligned} n_2^{\Xi^2}(t) + n_3^{\Xi^2}(t) + n_4^{\Xi^2}(t) + n_7^{\Xi^2}(t) + n_8^{\Xi^2}(t) = \\ \frac{1}{3} [4c_{20}^2 c_{20}^{*2} - 3c_{20}^* c_{30}^2 - 3c_{10}^{*2} (c_{20}^2 - c_{30}^2), \\ + 2c_{20} c_{20}^* c_{30} c_{30}^* - 3c_{20}^2 c_{30}^{*2} + 4c_{30}^2 c_{30}^{*2} + 2c_{10} c_{10}^* (c_{20} c_{20}^* + c_{30} c_{30}^*) \\ + c_{10}^2 (4c_{10}^{*2} - 3c_{20}^{*2} + 3c_{30}^{*2})], \end{aligned} \quad (34b)$$

and

$$\begin{aligned} n_1^{\Xi^2}(t) + n_5^{\Xi^2}(t) + n_6^{\Xi^2}(t) = c_{10}^{*2} (c_{20}^2 - c_{30}^2) + (c_{20}^* c_{30} + c_{20} c_{30}^*)^2 \\ + 2c_{10} c_{10}^* (c_{20} c_{20}^* + c_{30} c_{30}^*) + c_{10}^2 (c_{20}^{*2} - c_{30}^{*2}), \end{aligned} \quad (34c)$$

respectively.

## 4 Trajectories of the SU(3) Bloch vectors

We are now in a position to discuss the phase portraits of different configurations of the three-level system to examine the dynamics of the SU(3) Bloch vectors. For numerical studies, we work with the initial condition where all three levels are equally populated, i.e.,  $c_{10} = c_{20} = c_{30} = 1/\sqrt{3}$  at  $t = 0$ . For example, for  $\Lambda$  configuration, the norm of the four-sphere  $\mathbb{S}^4$  at zero detuning is given by,

$$n_2^2(t) + n_3^2(t) + n_5^2(t) + n_6^2(t) + n_8^2(t) = \frac{4}{9}, \quad (35a)$$

from Eq.(32b) and that for the two-sphere  $\mathbb{S}^2$  we have,

$$n_1^2(t) + n_4^2(t) + n_7^2(t) = \frac{8}{9}, \quad (35b)$$

from Eq.(32c).

Let us begin by considering the time-series plots of all Bloch vectors at resonance ( $\Delta = 0$ ) and off-resonance ( $\Delta \neq 0$ ), as shown in Figs.1-3 for the  $\Lambda$ ,  $V$  and  $\Xi$  configurations. The periodic behavior of the evolution curves at resonance ( $\Delta = 0$ ) is clearly evident from Figs.(1a,2a,3a). We note that this periodicity changes its pattern for the nonzero value ( $\Delta \neq 0$ ) of the detuning parameter shown in Figs.(1b,2b,3b).

To make the physical content of the dynamics more transparent, we now consider the phase space plots (i.e.,  $n_i(t)$  versus  $\dot{n}_i(t)$  plots) of the Bloch vectors shown in Fig.4-6 for three configurations (For a detailed derivation of  $n_i(t)$  and  $\dot{n}_i(t)$ , see Appendix A and B). At resonance, the phase portraits of three configurations reveal closed curves, signifying stable and periodic behavior of the Bloch trajectories. However, when a finite detuning is turned on, several Bloch vectors exhibit a noticeable precession, contrast to those seen at resonance. Thus it is worth noting that at zero detuning, the entire SU(3) Bloch sphere  $\mathbb{S}^7$  splits as into two sectors,  $\mathbb{S}^4$  and  $\mathbb{S}^2$  which are characterized by their distinctive Bloch trajectories. In Figures 4a,5a, and 6a, we have displayed the phase portrait of the  $\mathbb{S}^4$  sector for the  $\Lambda$  configuration ( $i = 2, 3, 5, 6, 8$ ), for the  $V$  configuration ( $i = 1, 3, 5, 7, 8$ ) and for the  $\Xi$  configuration ( $i = 2, 3, 4, 7, 8$ ), respectively. In particular we note that all configurations are closed and exhibit complex trisectrix family of curves with their characteristic looping and branching patterns. Such structure is highly sensitive to the system's parameters revealing the richness of underlying geometry and nontrivial topology of that sector. In Figures 4b,5b, and 6b, display the phase portraits of the  $\mathbb{S}^2$  sector for the  $\Lambda$  configuration ( $i = 1, 4, 7$ ), the  $V$  configuration ( $i = 2, 4, 6$ ) and the  $\Xi$  configurations ( $i = 1, 5, 6$ ). In contrast

to the previous sector, these plots for all configurations exhibits a trajectory that is closer to the ellipse at resonance and display a regular precessional feature at off-resonance.

## 5 Conclusions

In this paper, we have investigated the Bloch space of the qutrit system by studying the Bloch trajectories for different configurations of three-level system. From the geometric perspective, when such a system is parameterized with spherical polar coordinates, it leads to a Bloch seven-sphere  $\mathbb{S}^7$  with the norm  $4/3$  which exceeds 1. This parameterization further facilitates the existence of three distinct principal cardinal states along with their superposed states. We then proceed to evaluate the norm for each configuration from the dynamical consideration and show that it is in conformity with the norm obtained by the aforesaid geometric approach. In this approach, additionally, the Bloch seven-sphere  $\mathbb{S}^7$  is found to split into a four-sphere  $\mathbb{S}^4$  and a two-sphere  $\mathbb{S}^2$  at resonance. We have compared the time series and phase space plots of the  $SU(3)$  Bloch vectors of all three-level configurations at and off-resonance. For  $\mathbb{S}^4$  sector, the Bloch trajectory reveals closed but a complex, trisectrix class of closed orbits, while for the  $\mathbb{S}^2$  sector, we have approximately elliptical trajectory. On the other hand, at off-resonance, such splitting vanishes and all the orbits display a precessional motion. Such distinctive dynamics of the Bloch vectors is reflecting an intricate and nontrivial geometry of the Bloch space of the qutrit system which requires further exploration. The analysis presented here is limited to a narrow range of numerical parameters, but extending it to a broader parameter range could uncover additional dynamical features of high-dimensional quantum systems, which might have deeper geometrical implications.

## Acknowledgment

We thank Dr Sovik Roy for discussion on the properties of the trisectrix curves.

## Figure Captions:

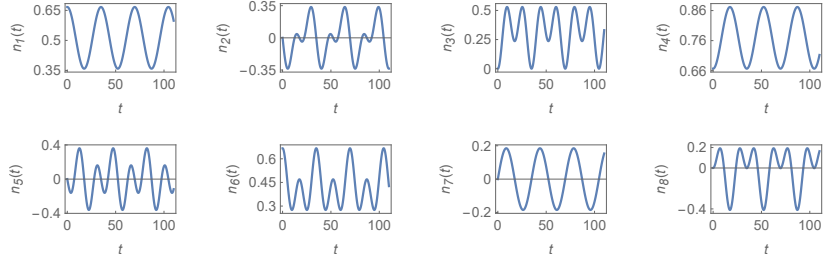


Fig1a: Time evolution of the SU(3) Bloch vectors  $n_i(t)$  at resonance ( $\Delta = 0$ ) for the  $\Lambda$  configuration with  $\kappa_{13} = .3$ ,  $\kappa_{23} = .2$  and  $c_1(0) = c_2(0) = c_3(0) = 1/\sqrt{3}$ .

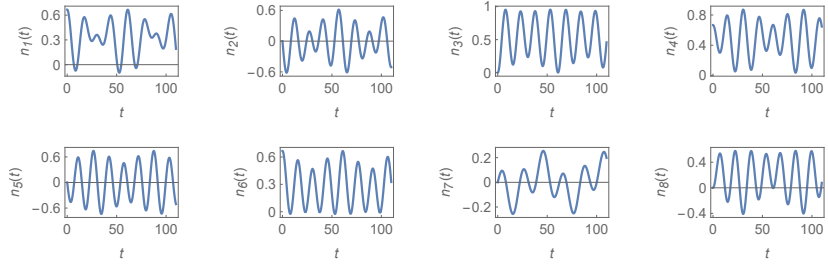


Fig1b: Time evolution of the SU(3) Bloch vectors at off-resonance ( $\Delta = .2$ ) for the  $\Lambda$  configuration with the same parameter values. The pattern of the periodic evolution of the Bloch vectors is found to be altered.

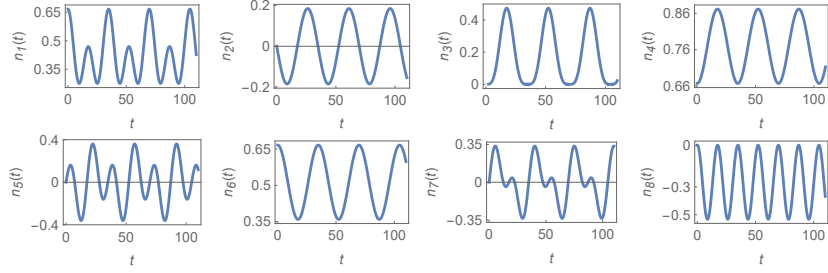


Fig2a: Time evolution of the SU(3) Bloch vectors  $n_i(t)$  at resonance ( $\Delta = 0$ ) for the  $V$  configuration with  $\kappa_{13} = .3$ ,  $\kappa_{12} = .2$  and  $c_1(0) = c_2(0) = c_3(0) = 1/\sqrt{3}$ .

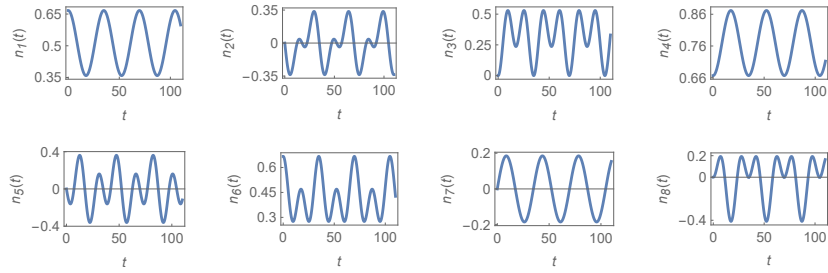


Fig2b: The time evolution of the Bloch vectors for the  $V$  configuration at off-resonance ( $\Delta = 0.2$ ) with same values of the parameters displays distinct pattern of periodicity.

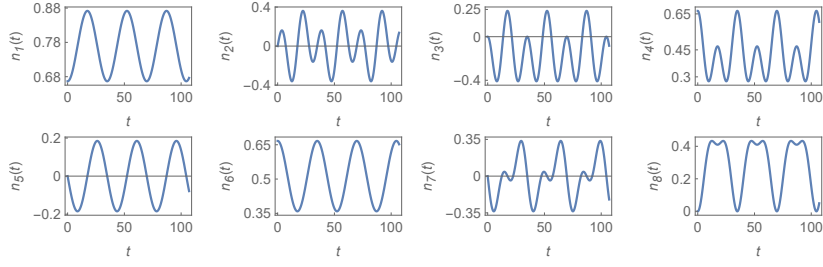


Fig3a: Time evolution of the Bloch vectors  $n_i(t)$  at resonance ( $\Delta = 0$ ) for the  $\Xi$  configuration with  $\kappa_{12} = .2$ ,  $\kappa_{23} = .3$ , and  $c_1(0) = c_2(0) = c_3(0) = 1/\sqrt{3}$ .

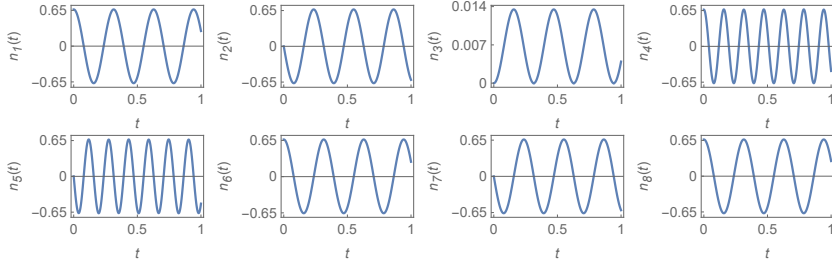


Fig3b: Time evolution of the SU(3) Bloch vectors at off-resonance for the  $\Xi$  configuration with same values of above parameters with detuning  $\Delta = 20$  showing distinct pattern of periodicity.



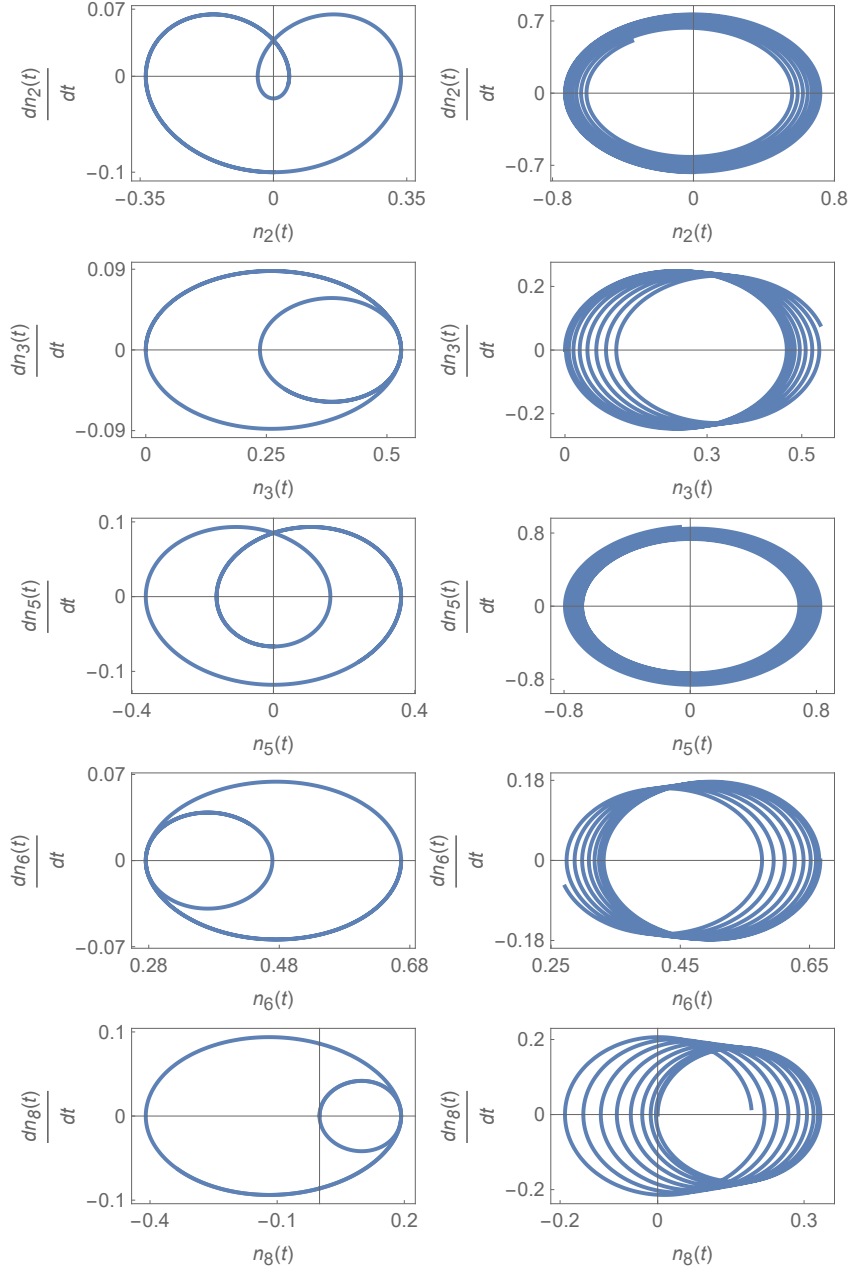


Fig.4a: Phase portraits of the SU(3) Bloch vectors  $n_i(t)$  ( $i = 2, 3, 5, 6, 8$ ) for the 4-sphere  $\mathbb{S}^4$  sector of the  $\Lambda$  configuration at resonance ( $\Delta = 0$ , Left column) are compared with those at off-resonance ( $\Delta = 1.2$ , Right column) with the parameters,  $\kappa_{13} = .3$ ,  $\kappa_{23} = .2$  and  $c_1(0) = c_2(0) = c_3(0) = 1/\sqrt{3}$ . The precession of the Bloch trajectories is clearly evident.

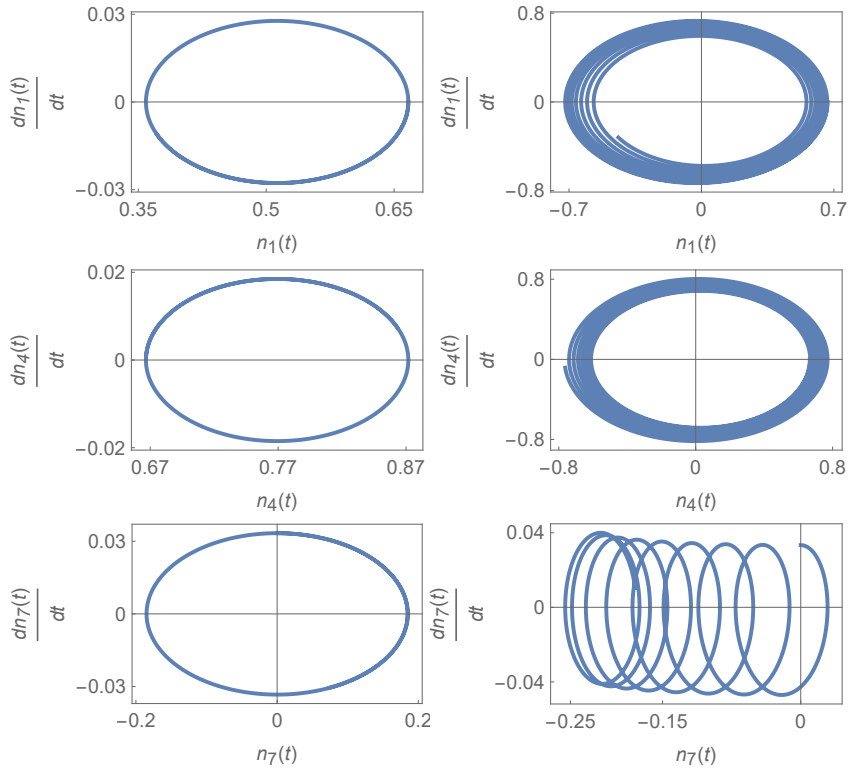


Fig.4b: The phase portrait of the SU(3) Bloch vectors  $n_i(t)$  ( $i = 1, 4, 7$ ) for the 2-sphere  $\mathbb{S}^2$  sector of the  $\Lambda$  configuration at resonance ( $\Delta = 0$ , Left column) and off-resonance ( $\Delta = 1.2$ , Right column) are compared using aforesaid parameters values.

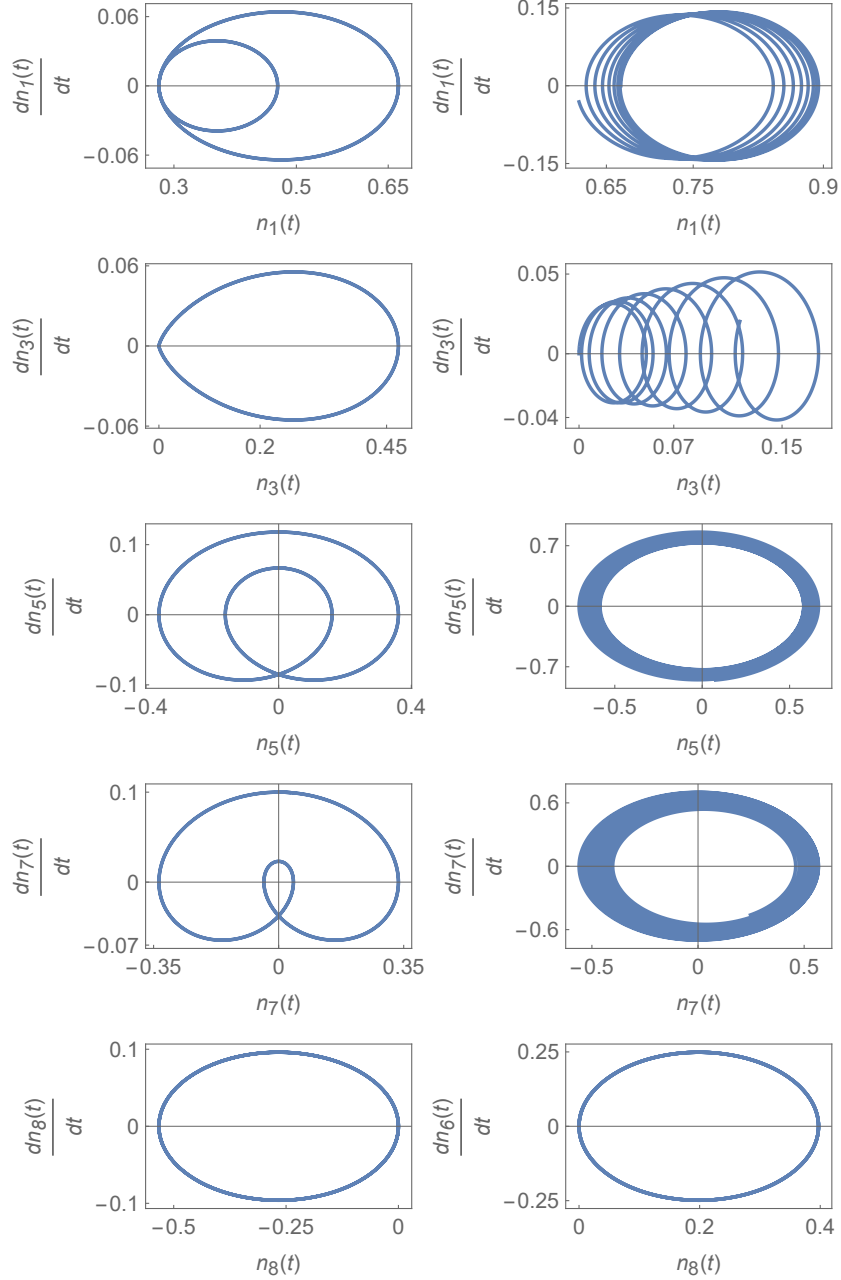


Fig.5a: Phase portraits of the SU(3) Bloch vectors  $n_i(t)$  ( $i = 1, 3, 5, 7, 8$ ) for the 4-sphere  $\mathbb{S}^4$  sector of the  $V$  configuration at resonance ( $\Delta = 0$ , Left column) are compared with those at off-resonance ( $\Delta = 0.2$ , Right column) with the parameters,  $\kappa_{13} = .3$ ,  $\kappa_{12} = .2$  and  $c_1(0) = c_2(0) = c_3(0) = 1/\sqrt{3}$ . The precession of the Bloch trajectories is clearly evident.

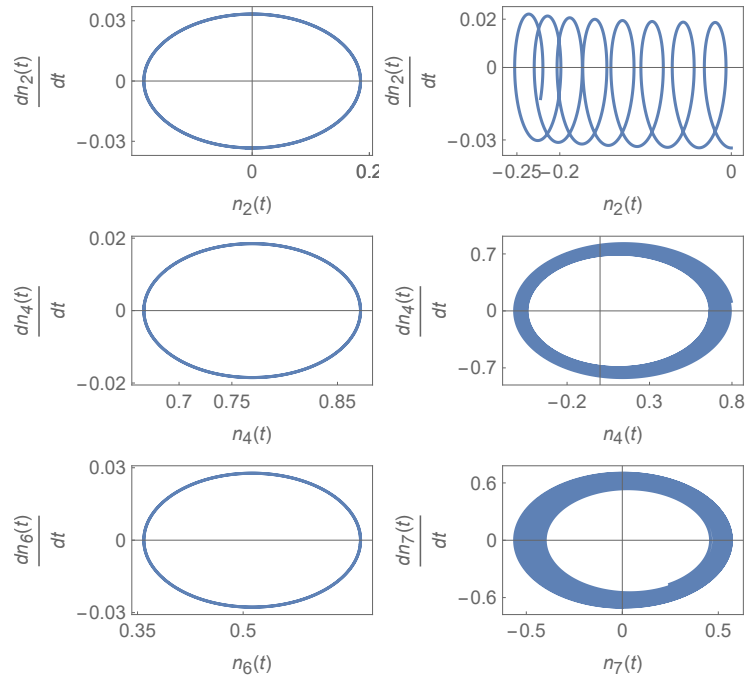


Fig.5b: The phase portrait of the SU(3) Bloch vectors  $n_i(t)$  ( $i = 2, 4, 6$ ) for the 2-sphere  $\mathbb{S}^2$  sector of the  $V$  configuration at resonance ( $\Delta = 0$ , Left column) and off-resonance ( $\Delta = 0.2$ , Right column) using the same parameter values.

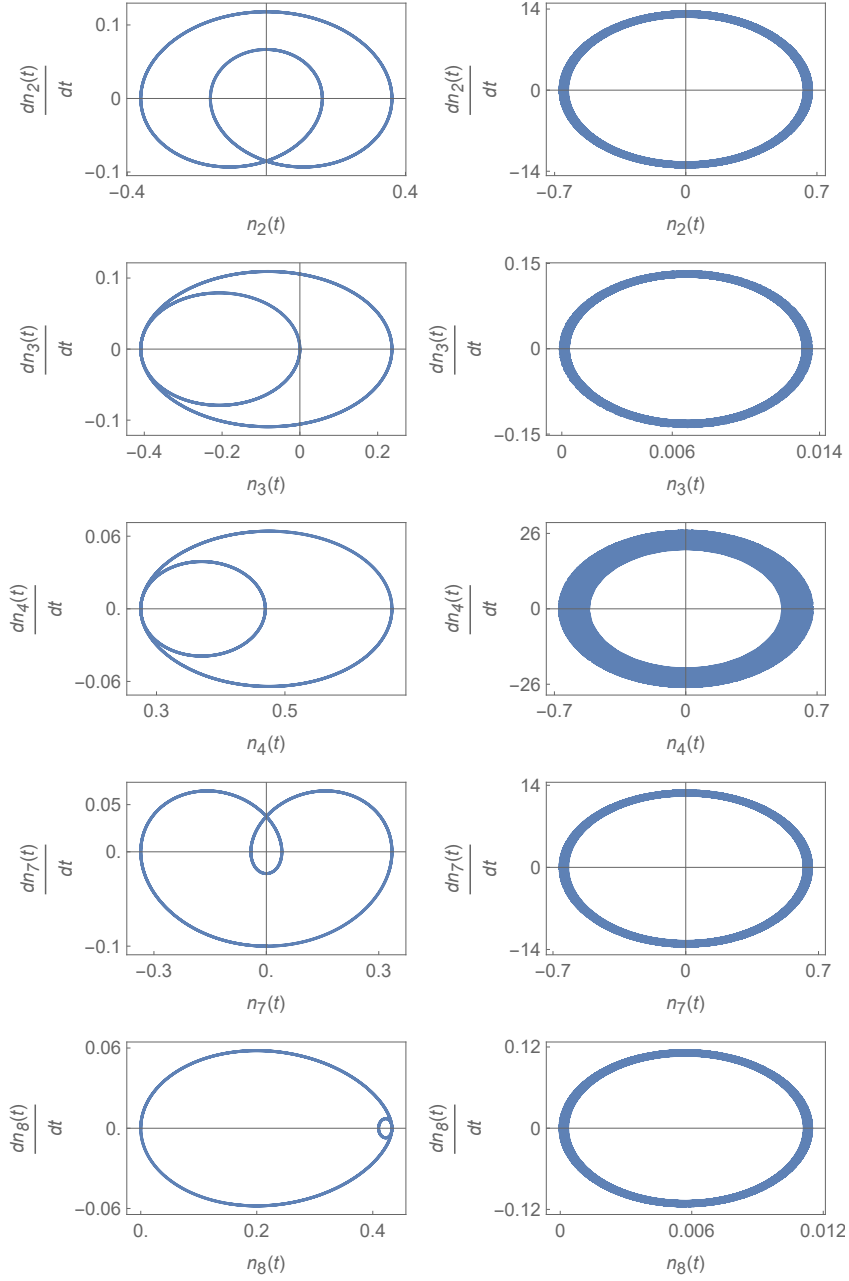


Fig.6a: Phase portrait of the SU(3) Bloch vectors  $n_i(t)$  ( $i = 2, 3, 5, 6, 8$ ) for the 4-sphere  $\mathbb{S}^4$  sector of the  $\Xi$  configuration at resonance ( $\Delta = 0$ , Left column) is compared with those at off-resonance ( $\Delta = 20$ , Right column) with  $\kappa_{12} = .2$ ,  $\kappa_{23} = .3$  and  $c_1(0) = c_2(0) = c_3(0) = 1/\sqrt{3}$ . Like previous two configurations, the Bloch trajectories exhibit a precession for the non-zero value of detuning.

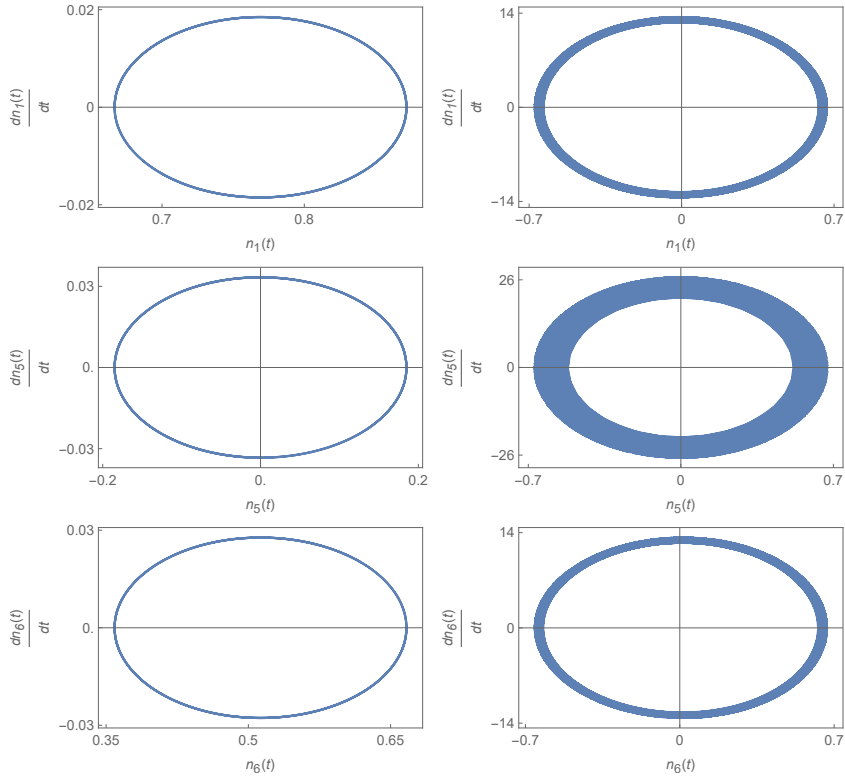


Fig.6b: The phase portrait of the SU(3) Bloch vectors  $n_i(t)$  ( $i = 1, 5, 6$ ) for the 2-sphere  $\mathbb{S}^2$  sector of the  $\Xi$  configuration at resonance ( $\Delta = 0$ , Left column) and off-resonance ( $\Delta = 20$ , Right column) which shows a precession at detuning  $\Delta = 20$ , using the same parameter values.

## Appendix A: SU(3) Bloch vectors for the $\Lambda$ configuration

The phase portrait of a given configurations requires the plotting of the phase plane coordinates  $(n_i(t), \dot{n}_i(t))$ . In this Appendix we have explicitly displayed the SU(3) Bloch vectors  $n_i(t)$  for the  $\Lambda$  configuration by plugging in the amplitudes from Eq.(24) into Eq.(31):

$$\begin{aligned}
n_1(t) = & \frac{e^{-i\frac{1}{2}\Delta t}}{(\kappa_{13}^2 + \kappa_{23}^2)\Omega^2} \left\{ e^{i\frac{1}{2}\Delta t} \kappa_{23} \left[ c_{10}(c_{10}^*\Delta + c_{30}^*\kappa_{13} + c_{20}^*\kappa_{23})(\kappa_{13}^2 + \kappa_{23}^2) \right. \right. \\
& + (c_{30}\kappa_{13} + c_{20}\kappa_{23})(-c_{30}^*\Delta\kappa_{13} - c_{20}^*\Delta\kappa_{23} + c_{10}^*(\kappa_{13}^2 + \kappa_{23}^2)) \left. \right] \\
& + \kappa_{13}(c_{20}^*\kappa_{13} - c_{30}^*\kappa_{23})\Omega \left[ c_{10}\Omega \cos\left(\frac{\Omega t}{2}\right) - i(c_{10}\Delta + c_{30}\kappa_{13} + c_{20}\kappa_{23}) \sin\left(\frac{\Omega t}{2}\right) \right] \\
& + e^{i\Delta t} \kappa_{13}(c_{20}\kappa_{13} - c_{30}\kappa_{23})\Omega \left[ c_{10}^*\Omega \cos\left(\frac{\Omega t}{2}\right) + i(c_{10}^*\Delta + c_{30}^*\kappa_{13} + c_{20}^*\kappa_{23}) \sin\left(\frac{\Omega t}{2}\right) \right] \\
& + e^{\frac{i\Delta t}{2}} \Delta\kappa_{23} \left[ \left( (c_{10}\Delta + c_{30}\kappa_{13} + c_{20}\kappa_{23})(c_{30}^*\kappa_{13} + c_{20}^*\kappa_{23}) \right. \right. \\
& + c_{10}^*(c_{30}\Delta\kappa_{13} + c_{20}\Delta\kappa_{23} - c_{10}(\kappa_{13}^2 + \kappa_{23}^2)) \left. \right) \cos \Omega t \\
& + i(c_{10}^*(c_{30}\kappa_{13} + c_{20}\kappa_{23}) - c_{10}(c_{30}^*\kappa_{13} + c_{20}^*\kappa_{23}))\Omega \sin \Omega t \left. \right] \left. \right\}, \quad (\text{A.1})
\end{aligned}$$

$$\begin{aligned}
n_2^\Lambda(t) = & \frac{1}{(\kappa_{13}^2 + \kappa_{23}^2)\Omega} \left\{ i e^{-\frac{i\Delta t}{2}} \kappa_{13} \left[ c_{10}^* e^{i\Delta t} (c_{20}\kappa_{13} - c_{30}\kappa_{23}) \right. \right. \\
& + c_{10}(-c_{20}^*\kappa_{13} + c_{30}^*\kappa_{23}) \left. \right] \Omega \cos\left(\frac{\Omega t}{2}\right) \\
& + \kappa_{23} \left[ c_{10}^*(c_{30}\kappa_{13} + c_{20}\kappa_{23}) - c_{10}(c_{30}^*\kappa_{13} + c_{20}^*\kappa_{23}) \right] \Omega \cos \Omega t \\
& + i e^{-\frac{i\Delta t}{2}} \kappa_{13} \left[ e^{i\Delta t} (c_{10}^*\Delta + c_{30}^*\kappa_{13} + c_{20}^*\kappa_{23})(c_{20}\kappa_{13} - c_{30}\kappa_{23}) \right. \\
& + (c_{10}\Delta + c_{30}\kappa_{13} + c_{20}\kappa_{23})(c_{20}^*\kappa_{13} - c_{30}^*\kappa_{23}) \left. \right] \sin\left(\frac{\Omega t}{2}\right) \\
& + i \kappa_{23} \left[ (c_{10}\Delta + c_{30}\kappa_{13} + c_{20}\kappa_{23})(c_{30}^*\kappa_{13} + c_{20}^*\kappa_{23}) \right. \\
& + c_{10}^*(c_{30}\Delta\kappa_{13} + c_{20}\Delta\kappa_{23} - c_{10}(\kappa_{13}^2 + \kappa_{23}^2)) \left. \right] \sin \Omega t \left. \right\}, \quad (\text{A.2})
\end{aligned}$$

$$\begin{aligned}
n_3^\Lambda(t) = & \frac{1}{2(\kappa_{13}^2 + \kappa_{23}^2)^2 \Omega^2} \left\{ \kappa_{13}^4 (c_{30} \kappa_{13} (c_{10}^* \Delta + c_{30}^* \kappa_{13}) - 2c_{20} c_{20}^* (\Delta^2 + \kappa_{13}^2)) \right. \\
& + \kappa_{13}^3 (2(c_{20}^* c_{30} + c_{20} c_{30}^*) \Delta^2 + c_{10}^* c_{20} \Delta \kappa_{13} + 3(c_{20}^* c_{30} + c_{20} c_{30}^*) \kappa_{13}^2) \kappa_{23} \\
& - \kappa_{13}^2 (4c_{30} c_{30}^* \Delta^2 - 3c_{10}^* c_{30} \Delta \kappa_{13} + (c_{20} c_{20}^* + c_{30} c_{30}^*) \kappa_{13}^2) \kappa_{23}^2 \\
& + \kappa_{13} (-2(c_{20}^* c_{30} + c_{20} c_{30}^*) \Delta^2 + 3c_{10}^* c_{20} \Delta \kappa_{13} + 3(c_{20}^* c_{30} + c_{20} c_{30}^*) \kappa_{13}^2) \kappa_{23}^3 \\
& + (2c_{30} \kappa_{13} (c_{10}^* \Delta - c_{30}^* \kappa_{13}) + c_{20} c_{20}^* (-2\Delta^2 + \kappa_{13}^2)) \kappa_{23}^4 \\
& + 2c_{10}^* c_{20} \Delta \kappa_{23}^5 \\
& + c_{10} (\kappa_{13}^2 + \kappa_{23}^2) \left[ c_{10}^* (2\Delta^2 + \kappa_{13}^2) (\kappa_{13}^2 + \kappa_{23}^2) \right. \\
& + \Delta (c_{30}^* \kappa_{13} + c_{20}^* \kappa_{23}) (\kappa_{13}^2 + 2\kappa_{23}^2) \left. \right] \\
& + 2\kappa_{13} \kappa_{23} \Omega \cos \left( \frac{\Delta t}{2} \right) \left[ (-c_{20}^* c_{30} + c_{20} c_{30}^*) \kappa_{13}^2 + 2(-c_{20} c_{20}^* + c_{30} c_{30}^*) \kappa_{13} \kappa_{23} \right. \\
& + (c_{20}^* c_{30} + c_{20} c_{30}^*) \kappa_{23}^2 \left. \right] \Omega \cos \left( \frac{\Omega t}{2} \right) \\
& + i (-c_{20}^* c_{30} \Delta + c_{20} c_{30}^* \Delta - c_{10}^* c_{20} \kappa_{13} + c_{10} c_{20}^* \kappa_{13} + c_{10}^* c_{30} \kappa_{23} - c_{10} c_{30}^* \kappa_{23}) \\
& \times (\kappa_{13}^2 + \kappa_{23}^2) \sin \left( \frac{\Omega t}{2} \right) \left. \right] \\
& + 2\kappa_{13} \kappa_{23} \Omega \sin \left( \frac{\Delta t}{2} \right) \left[ i (c_{20}^* c_{30} - c_{20} c_{30}^*) (\kappa_{13}^2 + \kappa_{23}^2) \Omega \cos \left( \frac{\Omega t}{2} \right) \right. \\
& + \left( \kappa_{13}^2 (-c_{20}^* c_{30} \Delta - c_{20} c_{30}^* \Delta + c_{10}^* c_{20} \kappa_{13} + c_{10} c_{20}^* \kappa_{13}) \right. \\
& - \kappa_{13} (2c_{20} c_{20}^* \Delta - 2c_{30} c_{30}^* \Delta + c_{10}^* c_{30} \kappa_{13} + c_{10} c_{30}^* \kappa_{13}) \kappa_{23} \\
& + (c_{20}^* c_{30} \Delta + c_{20} c_{30}^* \Delta + c_{10}^* c_{20} \kappa_{13} + c_{10} c_{20}^* \kappa_{13}) \kappa_{23}^2 - (c_{10}^* c_{30} + c_{10} c_{30}^*) \kappa_{23}^3 \left. \right] \\
& + (\kappa_{13}^2 + \kappa_{23}^2) (\kappa_{13}^2 + 2\kappa_{23}^2) \left[ - \left( (c_{10} \Delta + c_{30} \kappa_{13} + c_{20} \kappa_{23}) (c_{30}^* \kappa_{13} + c_{20}^* \kappa_{23}) \right. \right. \\
& + c_{10}^* (c_{30} \Delta \kappa_{13} + c_{20} \Delta \kappa_{23} - c_{10} (\kappa_{13}^2 + \kappa_{23}^2)) \cos \Omega t \left. \right) \\
& \left. - i (c_{10}^* (c_{30} \kappa_{13} + c_{20} \kappa_{23}) - c_{10} (c_{30}^* \kappa_{13} + c_{20}^* \kappa_{23})) \Omega \sin \Omega t \right] \left. \right\}, \quad (\text{A.3})
\end{aligned}$$



$$\begin{aligned}
n_4^\Lambda(t) &= \frac{e^{-\frac{1}{2}i\Delta t}}{(\kappa_{13}^2 + \kappa_{23}^2)\Omega^2} \\
&\times \left\{ \kappa_{23} \left( -c_{10}^* e^{i\Delta t} (\kappa_{20}\kappa_{13} - \kappa_{30}\kappa_{23}) + c_{10} (-c_{20}^* \kappa_{13} + c_{30s}\kappa_{23}) \right) \Omega^2 \cos\left(\frac{\Omega t}{2}\right) \right. \\
&+ i e^{i\Delta t} \kappa_{23} (c_{10}^* \Delta + c_{30s}\kappa_{13} + c_{20}^* \kappa_{23}) (-\kappa_{20}\kappa_{13} + \kappa_{30}\kappa_{23}) \Omega \sin\left(\frac{\Omega t}{2}\right) \\
&+ i \kappa_{23} (c_{10}\Delta + c_{30}\kappa_{13} + c_{20}\kappa_{23}) (c_{20}^* \kappa_{13} - c_{30s}\kappa_{23}) \Omega \sin\left(\frac{\Omega t}{2}\right) \\
&+ e^{\frac{i\Delta t}{2}} \kappa_{13} \left[ c_{10} (c_{10}^* \Delta + c_{30s}\kappa_{13} + c_{20}^* \kappa_{23}) (\kappa_{13}^2 + \kappa_{23}^2) \right. \\
&+ (c_{30}\kappa_{13} + c_{20}\kappa_{23}) (-c_{30s}\Delta\kappa_{13} - c_{20}^* \Delta\kappa_{23} + c_{10}^* (\kappa_{13}^2 + \kappa_{23}^2)) \\
&+ \Delta \left[ (c_{10}\Delta + c_{30}\kappa_{13} + c_{20}\kappa_{23}) (c_{30s}\kappa_{13} + c_{20}^* \kappa_{23}) \right. \\
&+ c_{10}^* (c_{30}\Delta\kappa_{13} + c_{20}\Delta\kappa_{23} - c_{10} (\kappa_{13}^2 + \kappa_{23}^2)) \left. \left. \right] \cos \Omega t \right. \\
&\left. + i \Delta (c_{10}^* (c_{30}\kappa_{13} + c_{20}\kappa_{23}) - c_{10} (c_{30s}\kappa_{13} + c_{20}^* \kappa_{23})) \Omega \sin \Omega t \right\}, \quad (\text{A.4})
\end{aligned}$$

$$\begin{aligned}
n_5^\Lambda(t) &= \frac{e^{-\frac{i\Delta t}{2}}}{(\kappa_{13}^2 + \kappa_{23}^2)\Omega} \\
&\times \left\{ i \kappa_{23} \left( -c_{10}^* e^{i\Delta t} (c_{20}\kappa_{13} - c_{30}\kappa_{23}) + c_{10} (c_{20}^* \kappa_{13} - c_{30}^* \kappa_{23}) \right) \Omega \cos\left(\frac{\Omega t}{2}\right) \right. \\
&+ e^{i\Delta t} \kappa_{23} (c_{10}^* \Delta + c_{30}^* \kappa_{13} + c_{20}^* \kappa_{23}) (c_{20}\kappa_{13} - c_{30}\kappa_{23}) \sin\left(\frac{\Omega t}{2}\right) \\
&+ \kappa_{23} (c_{10}\Delta + c_{30}\kappa_{13} + c_{20}\kappa_{23}) (c_{20}^* \kappa_{13} - c_{30}^* \kappa_{23}) \sin\left(\frac{\Omega t}{2}\right) \\
&+ e^{\frac{i\Delta t}{2}} \kappa_{13} \left( i (c_{10}^* (c_{30}\kappa_{13} + c_{20}\kappa_{23}) - c_{10} (c_{30}^* \kappa_{13} + c_{20}^* \kappa_{23})) \Omega \cos \Omega t \right. \\
&- \left. \left( (c_{10}\Delta + c_{30}\kappa_{13} + c_{20}\kappa_{23}) (c_{30}^* \kappa_{13} + c_{20}^* \kappa_{23}) \right) \right. \\
&\left. \left. + c_{10}^* (c_{30}\Delta\kappa_{13} + c_{20}\Delta\kappa_{23} - c_{10} (\kappa_{13}^2 + \kappa_{23}^2)) \right) \sin \Omega t \right\}, \quad (\text{A.5})
\end{aligned}$$

$$\begin{aligned}
n_6^\Lambda(t) = & \frac{1}{(\kappa_{13}^2 + \kappa_{23}^2)^2 \Omega^2} \left\{ \kappa_{13} \kappa_{23} \left( \kappa_{13}^2 \left( 2c_{30} c_{30}^* \Delta^2 - (c_{10}^* c_{30} + c_{10} c_{30}^*) \Delta \kappa_{13} \right. \right. \right. \\
& + (c_{10} c_{10}^* + c_{30} c_{30}^*) \kappa_{13}^2 - 2c_{20} c_{20}^* (\Delta^2 + \kappa_{13}^2) \Big) \\
& + \kappa_{13} \left( 4(c_{20}^* c_{30} + c_{20} c_{30}^*) \Delta^2 - (c_{10}^* c_{20} + c_{10} c_{20}^*) \Delta \kappa_{13} \right. \\
& + 3(c_{20}^* c_{30} + c_{20} c_{30}^*) \kappa_{13}^2 \Big) \kappa_{23} \\
& - \left( 2(-c_{20} c_{20}^* + c_{30} c_{30}^*) \Delta^2 + (c_{10}^* c_{30} + c_{10} c_{30}^*) \Delta \kappa_{13} \right. \\
& + (-2c_{10} c_{10}^* + c_{20} c_{20}^* + c_{30} c_{30}^*) \kappa_{13}^2 \Big) \kappa_{23}^2 \\
& - \left( c_{10}^* c_{20} \Delta + c_{10} c_{20}^* \Delta - 3(c_{20}^* c_{30} + c_{20} c_{30}^*) \kappa_{13} \right) \kappa_{23}^3 \\
& + (c_{10} c_{10}^* + c_{20} c_{20}^* - 2c_{30} c_{30}^*) \kappa_{23}^4 \Big) \\
& + (\kappa_{13} - \kappa_{23})(\kappa_{13} + \kappa_{23}) \Omega \cos \left( \frac{\Delta t}{2} \right) \left( (c_{20}^* c_{30} + c_{20} c_{30}^*) \kappa_{13}^2 \right. \\
& + 2(c_{20} c_{20}^* - c_{30} c_{30}^*) \kappa_{13} \kappa_{23} - (c_{20}^* c_{30} + c_{20} c_{30}^*) \kappa_{23}^2 \Big) \Omega \cos \left( \frac{\Omega t}{2} \right) \\
& + i(c_{20}^* c_{30} \Delta - c_{20} c_{30}^* \Delta + c_{10}^* c_{20} \kappa_{13} - c_{10} c_{20}^* \kappa_{13} \\
& - c_{10}^* c_{30} \kappa_{23} + c_{10} c_{30}^* \kappa_{23})(\kappa_{13}^2 + \kappa_{23}^2) \sin \left( \frac{\Omega t}{2} \right) \Big) \\
& + (\kappa_{13} - \kappa_{23})(\kappa_{13} + \kappa_{23}) \Omega \sin \left( \frac{\Delta t}{2} \right) \left( -i(c_{20}^* c_{30} - c_{20} c_{30}^*)(\kappa_{13}^2 + \kappa_{23}^2) \Omega \cos \left( \frac{\Omega t}{2} \right) \right. \\
& + \left( \kappa_{13}^2 (c_{20}^* c_{30} \Delta + c_{20} c_{30}^* \Delta - c_{10}^* c_{20} \kappa_{13} - c_{10} c_{20}^* \kappa_{13}) \right. \\
& + \kappa_{13} \left( 2c_{20} c_{20}^* \Delta - 2c_{30} c_{30}^* \Delta + c_{10}^* c_{30} \kappa_{13} + c_{10} c_{30}^* \kappa_{13} \right) \kappa_{23} \\
& - (c_{20}^* c_{30} \Delta + c_{20} c_{30}^* \Delta + c_{10}^* c_{20} \kappa_{13} + c_{10} c_{20}^* \kappa_{13}) \kappa_{23}^2 \\
& + (c_{10}^* c_{30} + c_{10} c_{30}^*) \kappa_{23}^3 \Big) \sin \left( \frac{\Omega t}{2} \right) \Big) \\
& + \kappa_{13} \kappa_{23} (\kappa_{13}^2 + \kappa_{23}^2) \left( (c_{10} \Delta + c_{30} \kappa_{13} + c_{20} \kappa_{23})(c_{30}^* \kappa_{13} + c_{20}^* \kappa_{23}) \right. \\
& + c_{10}^* (c_{30} \Delta \kappa_{13} + c_{20} \Delta \kappa_{23} - c_{10} (\kappa_{13}^2 + \kappa_{23}^2)) \Big) \cos \Omega t \\
& \left. + i \left( c_{10}^* (c_{30} \kappa_{13} + c_{20} \kappa_{23}) - c_{10} (c_{30}^* \kappa_{13} + c_{20}^* \kappa_{23}) \right) \Omega \sin \Omega t \right\} \quad (\text{A.6})
\end{aligned}$$

$$\begin{aligned}
n_7^\Lambda(t) = & \frac{1}{(\kappa_{13}^2 + \kappa_{23}^2)\Omega^2} \left\{ \Omega \sin\left(\frac{\Delta t}{2}\right) \left( (c_{20}^* c_{30} + c_{20} c_{30}^*) \kappa_{13}^2 \right. \right. \\
& + 2(c_{20} c_{20}^* - c_{30} c_{30}^*) \kappa_{13} \kappa_{23} - (c_{20}^* c_{30} + c_{20} c_{30}^*) \kappa_{23}^2 \Big) \Omega \cos\left(\frac{\Omega t}{2}\right) \\
& + i \left( c_{20}^* c_{30} \Delta - c_{20} c_{30}^* \Delta + c_{10}^* c_{20} \kappa_{13} - c_{10} c_{20}^* \kappa_{13} \right. \\
& \left. - c_{10}^* c_{30} \kappa_{23} + c_{10} c_{30}^* \kappa_{23} \right) (\kappa_{13}^2 + \kappa_{23}^2) \sin\left(\frac{\Omega t}{2}\right) \Big) \\
& + \Omega \cos\left(\frac{\Delta t}{2}\right) \left( i \left( c_{20}^* c_{30} - c_{20} c_{30}^* \right) (\kappa_{13}^2 + \kappa_{23}^2) \Omega \cos\left(\frac{\Omega t}{2}\right) \right. \\
& + \left( \kappa_{13}^2 \left( -c_{20}^* c_{30} \Delta - c_{20} c_{30}^* \Delta + c_{10}^* c_{20} \kappa_{13} + c_{10} c_{20}^* \kappa_{13} \right) \right. \\
& \left. - \kappa_{13} \left( 2c_{20} c_{20}^* \Delta - 2c_{30} c_{30}^* \Delta + c_{10}^* c_{30} \kappa_{13} + c_{10} c_{30}^* \kappa_{13} \right) \kappa_{23} \right. \\
& \left. + \left( c_{20}^* c_{30} \Delta + c_{20} c_{30}^* \Delta + c_{10}^* c_{20} \kappa_{13} + c_{10} c_{20}^* \kappa_{13} \right) \kappa_{23}^2 \right. \\
& \left. - (c_{10}^* c_{30} + c_{10} c_{30}^*) \kappa_{23}^3 \right) \sin\left(\frac{\Omega t}{2}\right) \Big) \Big\} \tag{A.7}
\end{aligned}$$

$$\begin{aligned}
n_8^\Lambda(t) = & \frac{1}{2\sqrt{3}(\kappa_{13}^2 + \kappa_{23}^2)^2\Omega^2} \left\{ \kappa_{13}^4 \left( 2(c_{10}c_{10}^* + c_{20}c_{20}^* - 2c_{30}c_{30}^*)\Delta^2 \right. \right. \\
& + 3(c_{10}^*c_{30} + c_{10}c_{30}^*)\Delta\kappa_{13} - (c_{10}c_{10}^* - 2c_{20}c_{20}^* + c_{30}c_{30}^*)\kappa_{13}^2 \Big) \\
& - 3\kappa_{13}^3 \left( 2(c_{20}^*c_{30} + c_{20}c_{30}^*)\Delta^2 - (c_{10}^*c_{20} + c_{10}c_{20}^*)\Delta\kappa_{13} \right. \\
& + (c_{20}^*c_{30} + c_{20}c_{30}^*)\kappa_{13}^2 \Big) \kappa_{23} \\
& + \kappa_{13}^2 \left( 4(c_{10}c_{10}^* - 2c_{20}c_{20}^* + c_{30}c_{30}^*)\Delta^2 + 3(c_{10}^*c_{30} + c_{10}c_{30}^*)\Delta\kappa_{13} \right. \\
& + 3(-c_{20}c_{20}^* + c_{30}c_{30}^*)\kappa_{13}^2 \Big) \kappa_{23}^2 \\
& + 3\kappa_{13} \left( 2(c_{20}^*c_{30} + c_{20}c_{30}^*)\Delta^2 + (c_{10}^*c_{20} + c_{10}c_{20}^*)\Delta\kappa_{13} \right. \\
& + (c_{20}^*c_{30} + c_{20}c_{30}^*)\kappa_{13}^2 \Big) \kappa_{23}^3 \\
& + \left( 2(c_{10}c_{10}^* + c_{20}c_{20}^* - 2c_{30}c_{30}^*)\Delta^2 + 3(c_{10}c_{10}^* - c_{20}c_{20}^*)\kappa_{13}^2 \right) \kappa_{23}^4 \\
& + 6(c_{20}^*c_{30} + c_{20}c_{30}^*)\kappa_{13}\kappa_{23}^5 + 2(c_{10}c_{10}^* + c_{20}c_{20}^* - 2c_{30}c_{30}^*)\kappa_{23}^6 \\
& + 3\kappa_{13} \left( 2\kappa_{23}\Omega \cos\left(\frac{\Delta t}{2}\right) \left[ (c_{20}^*c_{30} + c_{20}c_{30}^*)\kappa_{13}^2 + 2(c_{20}c_{20}^* - c_{30}c_{30}^*)\kappa_{13}\kappa_{23} \right. \right. \\
& \left. \left. - (c_{20}^*c_{30} + c_{20}c_{30}^*)\kappa_{23}^2 \right] \Omega \cos\left(\frac{\Omega t}{2}\right) \right. \\
& + i \left( c_{20}^*c_{30}\Delta - c_{20}c_{30}^*\Delta + c_{10}^*c_{20}\kappa_{13} - c_{10}c_{20}^*\kappa_{13} \right. \\
& \left. \left. - c_{10}^*c_{30}\kappa_{23} + c_{10}c_{30}^*\kappa_{23} \right) (\kappa_{13}^2 + \kappa_{23}^2) \sin\left(\frac{\Omega t}{2}\right) \right] \\
& + 2\kappa_{23}\Omega \sin\left(\frac{\Delta t}{2}\right) \left[ -i(c_{20}^*c_{30} - c_{20}c_{30}^*)(\kappa_{13}^2 + \kappa_{23}^2)\Omega \cos\left(\frac{\Omega t}{2}\right) \right. \\
& + \left( \kappa_{13}^2 (c_{20}^*c_{30}\Delta + c_{20}c_{30}^*\Delta - c_{10}^*c_{20}\kappa_{13} - c_{10}c_{20}^*\kappa_{13}) \right. \\
& + \kappa_{13} (2c_{20}c_{20}^*\Delta - 2c_{30}c_{30}^*\Delta + c_{10}^*c_{30}\kappa_{13} + c_{10}c_{30}^*\kappa_{13}) \kappa_{23} \\
& \left. \left. - (c_{20}^*c_{30}\Delta + c_{20}c_{30}^*\Delta + c_{10}^*c_{20}\kappa_{13} + c_{10}c_{20}^*\kappa_{13}) \kappa_{23}^2 \right. \right. \\
& \left. \left. + (c_{10}^*c_{30} + c_{10}c_{30}^*)\kappa_{23}^3 \right) \sin\left(\frac{\Omega t}{2}\right) \right] \\
& + \kappa_{13}(\kappa_{13}^2 + \kappa_{23}^2) \left[ - \left( (c_{10}\Delta + c_{30}\kappa_{13} + c_{20}\kappa_{23})(c_{30}^*\kappa_{13} + c_{20}^*\kappa_{23}) \right. \right. \\
& + c_{10}^* \left( c_{30}\Delta\kappa_{13} + c_{20}\Delta\kappa_{23} - c_{10}(\kappa_{13}^2 + \kappa_{23}^2) \right) \Big) \cos\Omega t \\
& \left. \left. - i \left( c_{10}^*(c_{30}\kappa_{13} + c_{20}\kappa_{23}) - c_{10}(c_{30}^*\kappa_{13} + c_{20}^*\kappa_{23}) \right) \Omega \sin\Omega t \right] \right\}, \tag{A.8}
\end{aligned}$$

where  $\Omega = \sqrt{\Delta^2 + \kappa_{13}^2 + \kappa_{23}^2}$ . The SU(3) Bloch vectors of the  $V$  and  $\Xi$  configurations can be obtained following same procedure.

## Appendix B: Bloch equation for $\Lambda$ , $V$ , and $\Xi$ configurations

To obtain the time derivative of the SU(3) Bloch vectors  $\dot{n}_i^A(t)$  ( $A = \Lambda, V, \Xi$ ), we shall make use of the Bloch equation of all three configurations and in this appendix we present their derivation:

### i) $\Lambda$ configuration:

For the  $\Lambda$  configuration, we consider their time derivative of Eq.(30),

$$\frac{dn^\Lambda(t)}{dt} = Tr \left[ \boldsymbol{\lambda} \frac{d\rho_{\text{TLS}}^\Lambda}{dt} \right]. \quad (\text{A.9})$$

Using the Liouville equation, namely,

$$\frac{d\rho_{\text{TLS}}^\Lambda(t)}{dt} = -i[\rho_{\text{TLS}}^\Lambda(t), H_{\text{R}}^\Lambda(0)], \quad (\text{A.10})$$

and the Hamiltonian Eq.(16), it is straightforward to obtain the desired Bloch equation of the  $\Lambda$  configuration (We choose the equal detuning condition, namely,  $\Delta_{13}^\Lambda = \Delta_{23}^\Lambda = \Delta^\Lambda$ ):

$$\frac{dn_1^\Lambda(t)}{dt} = -\Delta^\Lambda n_2^\Lambda(t) - \frac{1}{2}\kappa_{13}n_7^\Lambda(t), \quad (\text{A.11a})$$

$$\frac{dn_2^\Lambda(t)}{dt} = \Delta^\Lambda n_1^\Lambda(t) + \kappa_{23}n_3^\Lambda(t) - \frac{1}{2}\kappa_{13}n_6^\Lambda(t), \quad (\text{A.11b})$$

$$\frac{dn_3^\Lambda(t)}{dt} = -\kappa_{23}n_2^\Lambda(t) - \frac{1}{2}\kappa_{13}n_5^\Lambda(t), \quad (\text{A.11c})$$

$$\frac{dn_4^\Lambda(t)}{dt} = -\Delta^\Lambda n_5^\Lambda(t) + \frac{1}{2}\kappa_{23}n_7^\Lambda(t), \quad (\text{A.11d})$$

$$\frac{dn_5^\Lambda(t)}{dt} = \frac{1}{2}\kappa_{13}n_3^\Lambda(t) + \Delta^\Lambda n_4^\Lambda(t) - \frac{1}{2}\kappa_{23}n_6^\Lambda(t) + \frac{1}{2}\sqrt{3}\kappa_{13}n_8^\Lambda(t), \quad (\text{A.11e})$$

$$\frac{dn_6^\Lambda(t)}{dt} = \frac{1}{2}\kappa_{13}n_2^\Lambda(t) + \frac{1}{2}\kappa_{23}n_5^\Lambda(t), \quad (\text{A.11f})$$

$$\frac{dn_7^\Lambda(t)}{dt} = \frac{1}{2}\kappa_{13}n_1^\Lambda(t) - \frac{1}{2}\kappa_{23}n_4^\Lambda(t), \quad (\text{A.11g})$$

$$\frac{dn_8^\Lambda(t)}{dt} = \frac{1}{2}\sqrt{3}\kappa_{13}n_5^\Lambda(t), \quad (\text{A.11h})$$

The time derivative of the Bloch vectors  $\dot{n}_i^A(t)$  can be obtained by substituting the Bloch vectors from Eqs.(A.1-A.8) into the right side of Eqs.(A.11a-A.11h). The procedure is similar for the other two configurations and for completeness, we have outlined the derivation of the Bloch vectors in the remaining sections of the Appendix.

## ii) $V$ configuration:

The unitary operator for the  $V$  configuration is given by,

$$U_V(t) = \exp \left[ -\frac{i}{3} \left( (2\Delta_{13} - \Delta_{12})V_3t + (2\Delta_{12} - \Delta_{13})U_3t \right) \right], \quad (\text{A.12})$$

and the corresponding Hamiltonian is given by,

$$\begin{aligned} \hat{H}_R^V(0) &= -iU_\Lambda^\dagger(t)U_V(t) + U_V^\dagger(t)\hat{H}^V(t)U_V(t) \\ &= \begin{bmatrix} \frac{1}{3}(2\Delta_{13} - \Delta_{12}) & 0 & \kappa_{13} \\ 0 & \frac{1}{3}(2\Delta_{12} - \Delta_{13}) & \kappa_{12} \\ \kappa_{13} & \kappa_{12} & -\frac{1}{3}(\Delta_{13} + \Delta_{12}), \end{bmatrix}. \end{aligned} \quad (\text{A.13})$$

where,  $\Delta_{12} = 2\omega_{12} + \omega_{13} - \Omega_{12}$  and  $\Delta_{13} = 2\omega_{13} + \omega_{12} - \Omega_{13}$  for the  $V$  configuration, respectively. Proceeding similar way we obtain the Bloch equation for the  $V$  configuration,

$$\frac{dn_1^V(t)}{dt} = -\kappa_{12}n_5^V(t) - \kappa_{13}n_7^V(t), \quad (\text{A.14a})$$

$$\frac{dn_2^V(t)}{dt} = \kappa_{12}n_4^V(t) - \kappa_{13}n_6^V(t), \quad (\text{A.14b})$$

$$\frac{dn_3^V(t)}{dt} = -\kappa_{13}n_5^V(t) + \kappa_{12}n_7^V(t), \quad (\text{A.14c})$$

$$\frac{dn_4^V(t)}{dt} = -\kappa_{12}n_2^V(t) + \Delta^V n_5^V(t), \quad (\text{A.14d})$$

$$\frac{dn_5^V(t)}{dt} = \kappa_{12}n_1^V(t) + \kappa_{13}n_3^V(t) - \Delta^V n_5^V(t) + \sqrt{3}\kappa_{13}n_8^V(t), \quad (\text{A.14e})$$

$$\frac{dn_6^V(t)}{dt} = \kappa_{13}n_2^V(t) + \Delta^V n_7^V(t), \quad (\text{A.14f})$$

$$\frac{dn_7^V(t)}{dt} = \kappa_{13}n_1^V(t) - \kappa_{12}n_3^V(t) - \Delta^V n_6^V(t) + \sqrt{3}\kappa_{12}n_8^V(t), \quad (\text{A.14g})$$

$$\frac{dn_8^V(t)}{dt} = -\sqrt{3}\kappa_{13}n_5^V(t) - \sqrt{3}\kappa_{12}n_7^V(t), \quad (\text{A.14h})$$

### iii) $\Xi$ configuration:

Finally for the  $\Xi$  configuration using the unitary operator,

$$U_{\Xi}(t) = \exp \left[ -\frac{i}{3} \left( (2\Delta_{12} + \Delta_{23})U_3t + (\Delta_{12} + 2\Delta_{23})T_3t \right) \right], \quad (\text{A.15})$$

we obtain the Hamiltonian of the  $\Xi$  configuration,

$$\begin{aligned} \hat{H}_{\text{R}}^{\Xi}(0) &= -i\dot{U}_{\Xi}^{\dagger}(t)U_{\Xi}(t) + U_{\Xi}^{\dagger}(t)H^{\Xi}(t)U_{\Xi}(t) \\ &= \begin{bmatrix} \frac{1}{3}(\Delta_{12} + 2\Delta_{23}) & \kappa_{23} & 0 \\ \kappa_{23} & \frac{1}{3}(\Delta_{12} - \Delta_{23}) & \kappa_{12} \\ 0 & \kappa_{12} & -\frac{1}{3}(2\Delta_{12} + \Delta_{23}) \end{bmatrix}. \end{aligned} \quad (\text{A.16})$$

where the detuning are given by  $\Delta_{12} = 2\omega_{12} + \omega_{23} - \Omega_{21}$  and  $\Delta_{23} = 2\omega_{23} + \omega_{32} - \Omega_{32}$ , respectively. The corresponding Bloch equations are given by,

$$\frac{dn_1^{\Xi}(t)}{dt} = \Delta^{\Xi}n_2^{\Xi}(t) - \frac{1}{2}\kappa n_5^{\Xi}(t), \quad (\text{A.17a})$$

$$\frac{dn_2^{\Xi}(t)}{dt} = \Delta^{\Xi}n_1^{\Xi}(t)2\kappa n_3^{\Xi}(t) + \frac{1}{2}\kappa n_4^{\Xi}(t) \quad (\text{A.17b})$$

$$\frac{dn_3^{\Xi}(t)}{dt} = -2\kappa n_2^{\Xi}(t) + \frac{1}{2}\kappa n_7^{\Xi}(t), \quad (\text{A.17c})$$

$$\frac{dn_4^{\Xi}(t)}{dt} = \frac{1}{2}\kappa n_2^{\Xi}(t) + \Delta^{\Xi}n_5^{\Xi}(t) + \frac{1}{2}\kappa n_7^{\Xi}(t), \quad (\text{A.17d})$$

$$\frac{dn_5^{\Xi}(t)}{dt} = \frac{1}{2}\kappa n_1^{\Xi}(t) - 2\Delta^{\Xi}n_4^{\Xi}(t) - \frac{1}{2}\kappa n_6^{\Xi}(t), \quad (\text{A.17e})$$

$$\frac{dn_6^{\Xi}(t)}{dt} = \frac{1}{2}\kappa n_5^{\Xi}(t) + \Delta^{\Xi}n_7^{\Xi}(t), \quad (\text{A.17f})$$

$$\frac{dn_7^{\Xi}(t)}{dt} = -\frac{1}{2}\kappa n_3^{\Xi}(t) - \frac{1}{2}\kappa n_4^{\Xi}(t) - \Delta^{\Xi}n_6^{\Xi}(t) + \frac{1}{2}\sqrt{3}\kappa n_8^{\Xi}(t), \quad (\text{A.17g})$$

$$\frac{dn_8^{\Xi}(t)}{dt} = -\frac{1}{2}\sqrt{3}\kappa n_7^{\Xi}(t), \quad (\text{A.17h})$$

where we have chosen equal value of the coupling parameters,  $\kappa_{12} = \kappa_{23} = \kappa$  for the equidistant  $\Xi$  configuration (i.e., ladder configuration).

## References

- [1] P. W. Milonni and J. H. Eberly. *Laser Physics*. Wiley, Hoboken, NJ, 2010.
- [2] M. A. Nielsen and I. L. Chuang. *Quantum Information and Quantum Computation*. Cambridge University Press, Cambridge, 10th edition, 2010.
- [3] G. Benenti, G. Casati, and G. Strini. *Principles of Quantum Computation and Information - Volume I: Basic Concepts and Volume II: Basic Tools and Special Topics*. World Scientific, Singapore, 1st edition, 2004.
- [4] G. Jaeger. *Quantum Information: An Overview*. Springer, Berlin, Heidelberg, 1st edition, November 2006.
- [5] S. K. Goyal, B. N. Simon, R. Singh, and S. Simon. Geometry of the generalized bloch sphere for qutrits. *Journal of Physics A: Mathematical and Theoretical*, **49**:165–203, March 2016.
- [6] A. Kossakowski and G. Kimura. The bloch-vector space for n-level systems: The spherical-coordinate point of view. *Open Systems & Information Dynamics*, **12**:207–229, 2005.
- [7] S. Zachcial and M. Zachcial. Alternative representation of  $n \times n$  density matrix. *Applied Physics B: Lasers and Optics*, **82**:143–151, March 2006.
- [8] R. A. Bertlmann and P. Krammer. Bloch vectors for qudits. *Journal of Physics A: Mathematical and Theoretical*, **41**:235–303, May 2008.
- [9] Arvind, K.S. Malleš, and N. Mukunda. The bloch vector for n-level systems. *Physics Letters A*, **314**:339–349, August 2003.
- [10] G. Kimura. The bloch vector for n-level systems. *Physics Letters A*, **314**:339–349, 2008.
- [11] L. Jakóbczyk and M. Siennicki. Geometry of bloch vectors in two-qubit system. *Physics Letters A*, **286**:383–390, 2001.
- [12] J. E. Avron, G. Bisker, and O. Kenneth. Visualizing two qubits. *Journal of Mathematical Physics*, **48**:102107, 2007.
- [13] S. Morelli, C. Eltschka, M. Huber, and J. Siewert. Correlation constraints and the bloch geometry of two qubits. *Quantum*, **7**:1027, 2023.



- [14] C. Wie. Bloch sphere model for two-qubit pure states. *arXiv preprint* , 2014. <https://arxiv.org/abs/1403.8069>.
- [15] J. Bley, E. Rexigel, A. Arias, N. Longen, L. Krupp, Ma. Kiefer-Emmanouilidis, P. Lukowicz, A. Donhauser, S. Küchemann, J. Kuhn, and A. Widera. Visualizing entanglement in multiqubit systems. *Physical Review Research*, **6**(2):023–077, 2024.
- [16] K. B. Wharton and D. Koch. Unit quaternions and the bloch sphere. *Journal of Physics A: Mathematical and Theoretical*, **48**:235–302, 2015.
- [17] A Ali, Paul Erker, Marcus Huber, and Claude Klöckl. Heisenberg-weyl observables: Bloch vectors in phase space. *Physical Review A*, **94**:010301, July 2016.
- [18] G. Sharma, S. Ghosh, and S. K. Sazim. Bloch sphere analog of qudits using heisenberg-weyl operators. *Physica Scripta*, **99**:045105, 2024.
- [19] B. Baumgartner, B. C. Hiesmayr, and Heide Narnhofer. State space for two qutrits has a phase space structure in its core. *Physical Review A*, **74**:032327, September 2006.
- [20] P. Kurzyński. Multi-bloch vector representation of the qutrit. *Journal of Physics A: Mathematical and Theoretical*, **44**:492–002, 2011.
- [21] I. Bengtsson and K. Życzkowski. *Geometry of Quantum States: An Introduction to Quantum Entanglement*. Cambridge University Press, Cambridge, UK, 2nd edition, 2017.
- [22] Bin Li, Zu-Huan Yu, and Shao-Ming Fei. Geometry of quantum computation with qutrits. *Scientific Reports*, **3**:2594, September 2013.
- [23] P. Kurzyński, A. Kołodziejcki, W. Laskowski, and M. Markiewicz. Three-dimensional visualization of a qutrit. *Physical Review A*, **93**:062126, 2016.
- [24] P. Kurzyński. Multi-bloch vector representation of the qutrit. *Quantum Information & Computation*, **11**:361–373, 2011.
- [25] S. Sen and T. K. Dey. An inequality for entangled qutrits in  $su(3)$  basis. *Quantum Information Processing*, **23**:267(1–12), 2024.
- [26] F. T. Hioe and J. H. Eberly. Nonlinear constants of motion for three-level quantum systems. *Physical Review A*, **25**:2168–2183, 1982.

- [27] F. T. Hioe. Gell-mann dynamic symmetry for n-level quantum systems. *Physical Review A*, 32:2824–2836, 1985.
- [28] H. I. Yoo and J. H. Eberly. Dynamical theory of an atom with two or three levels interacting with quantized cavity fields. *Physics Reports*, 118:239–337, 1985.
- [29] M. R. Nath, S. Sen, A. K. Sen, and G. Gangopadhyay. Bloch space structure, the qutrit wavefunction, and atom–field entanglement in three-level systems. *Pramana - Journal of Physics*, **71**:77–97, July 2008.
- [30] S. Sen, M. R. Nath, T. K. Dey, and Gautam Gangopadhyay. Bloch space structure, the qutrit wavefunction, and atom–field entanglement in three-level systems. *Annals of Physics*, **327**:224–252, 2012.
- [31] S. Sen, T. K. Dey, and B. Deb. A unified approach to lambda, cascade, and vee-type systems with one continuum. *Journal of Modern Optics*, **64**:2083–2096, July 2017.
- [32] S. Sen, T. K. Dey, and B. Deb. Resonance fluorescence in lambda, cascade, and vee type three-level configurations. *Physica Scripta*, **98**:115–124, 2023.
- [33] S. Sen, M. R. Nath, T. K. Dey, and Gautam Gangopadhyay. Bloch space structure, the qutrit wavefunction, and atom–field entanglement in three-level systems. *Annals of Physics*, **327**:224–252, 2012.
- [34] W. Greiner and B. Müller. *Quantum Mechanics: Symmetries*. Springer Science and Business Media, New York, 2012.
- [35] Wikipedia. Quantum mechanics — Wikipedia, the free encyclopedia. <http://en.wikipedia.org/w/index.php?title=Quantum%20mechanics&oldid=1258667380>, 2024. [Online; accessed 24-November-2024].